



HHS Public Access

Author manuscript

J Physiol. Author manuscript; available in PMC 2023 November 01.

Published in final edited form as:

J Physiol. 2022 November ; 600(22): 4897–4916. doi:10.1113/JP283605.

Properties and modulation of excitatory inputs to the locus coeruleus

Kelsey Barcomb¹, Samantha S Olah¹, Matthew J Kennedy¹, Christopher P Ford^{*1}

¹Department of Pharmacology, University of Colorado School of Medicine, Anschutz Medical Campus, Aurora, CO 80045, USA

Abstract

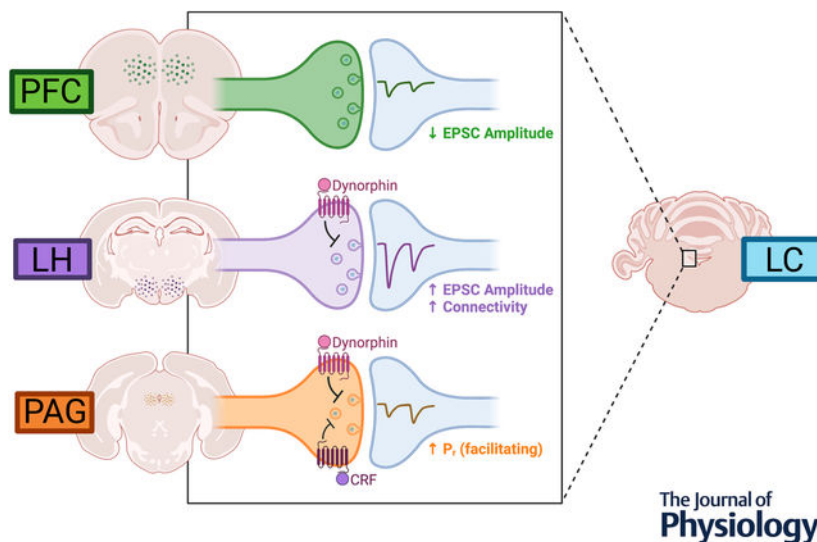
Excitatory inputs drive burst firing of locus coeruleus (LC) norepinephrine (NE) neurons in response to a variety of stimuli. Though a small number of glutamatergic LC afferents have been investigated, the overall landscape of these excitatory inputs is largely unknown. The current study used an optogenetic approach to isolate three glutamatergic afferents: the prefrontal cortex (PFC), the lateral hypothalamus (LH) and periaqueductal grey (PAG). AAV5-DIO-ChR2 was injected into each region in male and female CaMKII-Cre mice and the properties of excitatory inputs on LC-NE cells were measured. Notably we found differences among these inputs. First, the pattern of axonal innervation differed between inputs such that LH afferents were concentrated in the posterior portion of the LC-NE somatic region while PFC afferents were denser in the medial dendritic region. Second, basal intrinsic properties varied for afferents, with LH inputs having the highest connectivity and the largest amplitude excitatory postsynaptic currents (EPSCs) while PAG inputs had the lowest initial release probability. Third, while orexin and oxytocin had minimal effects on any input, dynorphin strongly inhibited excitatory inputs originating from the LH and PAG, and corticotrophin releasing factor (CRF) selectively inhibited inputs from the PAG. Overall, these results demonstrate that individual afferents to the LC have differing properties, which may contribute to the modularity of the LC and its ability to mediate various behavioral outcomes.

Graphical Abstract

***Lead / Corresponding author:** Christopher Ford (christopher.ford@cuanschutz.edu), **Address for Correspondence:** Department of Pharmacology, University of Colorado School of Medicine, 12800 E 19th Ave, Aurora, CO, 80045.

Author Contributions: All experiments were performed in the lab of CPF. KB and CPF designed experiments. KB performed all experiments. SSO and MJK assisted with synaptophysin labeled puncta image analysis. KB and CPF wrote the manuscript. All authors approved the final version of the manuscript; agree to be accountable for all aspects of the work in ensuring that questions related to the accuracy or integrity of any part of the work are appropriately investigated and resolved; and all persons designated as authors qualify for authorship, and all those who qualify for authorship are listed.

Competing interests: The authors declare no competing interests.



Norepinephrine (NE) neurons in the locus coeruleus (LC) receive glutamatergic inputs from various regions of the brain that drive their activity. In order to characterize how these afferents differ from one another with respect to synaptic properties, an optogenetic approach was used to isolate inputs from three specific regions: lateral hypothalamus (LH), periaqueductal grey (PAG), and prefrontal cortex (PFC). CaMKII-Cre mice were injected with channelrhodopsin into these target afferents and optically-evoked excitatory postsynaptic currents (EPSCs) were recorded from LC-NE cells using whole-cell slice electrophysiology. We found that basally, EPSCs from PFC afferents had the lowest amplitude. LH inputs conversely had the highest amplitude and also the highest probability of connectivity. PAG inputs were similar in size to PFC, though they were facilitatory indicating a higher release probability. Further exploring these connections in the context of neuromodulation, we found that only LH and PAG inputs were sensitive to dynorphin-induced synaptic depression. PFC afferents were unaffected by dynorphin treatment. The PAG inputs were also sensitive to CRF, exhibiting a slight depression in the presence of the peptide, which was not observed in LH or PFC inputs. These results overall show that different glutamatergic afferents to the LC have unique properties that may result in differential influences on LC-NE activity.

INTRODUCTION

The locus coeruleus (LC) consists of a dense cluster of norepinephrine (NE) neurons projecting widely throughout the brain and spinal cord (Berridge and Waterhouse, 2003; Jones and Moore, 1977; Sara, 2009). These cells serve as the primary source of NE to the brain and regulate a wide array of behaviors including arousal, attention, sensory gating, pain, and stress (Foote et al., 1991). This ability to mediate such diverse behaviors is not fully understood, though it is proposed to involve a modular organization of the LC that is generated by efferent specificity as well as activity-dependent recruitment of specific LC inputs (Chandler et al., 2019). A more thorough description of these inputs is required for a full picture of this modularity.

Through mapping of the afferent inputs to the LC, studies suggest that LC-NE neurons receive input from many regions (Aston-Jones et al., 1991; Cedarbaum and Aghajanian, 1978; Luppi et al., 1995; Schwarz et al., 2015). LC-NE neurons are tonically active, with the rate of activity linked to arousal and attention (Aston-Jones and Bloom, 1981; Foote et al., 1980). They also exhibit burst firing dependent on glutamatergic signaling, especially in response to noxious stimuli (Akaoka and Aston-Jones, 1991; Ennis and Aston-Jones, 1988; Ennis et al., 1992; Hajós and Engberg, 1990; Page et al., 1992). The source of glutamate has historically been attributed to only a few regions (Aston-Jones et al., 1986), primarily the medial prefrontal cortex (PFC) (Jodo and Aston-Jones, 1997) and the paraventricular nucleus of the ventrolateral medulla (Ennis et al., 1992). However, other regions have been identified based on fractional input density as having relatively strong LC afferents (Schwarz et al., 2015) but have not been widely explored in regard to their synaptic connectivity. The lateral hypothalamus (LH) is known to exert an excitatory influence over the LC (Sears et al., 2013) and a subpopulation of LH cells are glutamatergic projection neurons (Godfrey and Borgland, 2019; Poller et al., 2013). The periaqueductal grey (PAG) sends a particularly dense afferent to the LC (Lopes et al., 2016; Mantyh, 1983) and its lateral region has been shown excite LC-NE neurons (Ennis et al., 1991). Little work however has focused on identifying and comparing the properties of other excitatory LC inputs, though a better description of these afferents would allow for a deeper understanding as to how the LC is able to integrate information originating from various sources.

While glutamate release in the LC leads to burst firing, neuromodulatory peptides influence the tonic firing rate of LC-NE neurons (Van Bockstaele and Valentino, 2013; Zitnik, 2016). Some of these peptides are associated with specific LC-related behaviors. Corticotropin releasing factor (CRF) and dynorphin are both released in the LC in response to stress (Curtis et al., 1993, 1997; Kreibich et al., 2008; McCall et al., 2015) while orexin A (OxA) is linked to arousal (Bourgin et al., 2000; Carter et al., 2010, 2012; Gompf and Aston-Jones, 2008). Other peptides, such as oxytocin (OT), are present in the LC but do not have a well-defined function (Hawthorn et al., 1984; Ostrowski, 1998; Petersson et al., 1998; Rosen et al., 2008). In addition to driving the activity of LC-NE neurons, there is evidence that several peptides including CRF, dynorphin, OxA and OT may modulate LC glutamatergic synapses (Hooshmand et al., 2019; Kodama and Kimura, 2002; Kreibich et al., 2008; Prouty et al., 2017; Wang et al., 2021). When and how these changes occur however is not well understood, including whether they display input-specificity.

In the current study, we used a viral-mediated optogenetic approach to isolate and compare LC afferents. The well-known glutamatergic afferent of the PFC was compared to the LH and PAG, two regions suggested to positively regulate the LC but not yet examined in this context. We found that the PFC, PAG, and LH all form monosynaptic glutamatergic connections with LC-NE neurons. These inputs had differing basal properties, consistent with a model by which they are able to differentially drive LC activity. Importantly, they displayed differences related to regulation by dynorphin and CRF, allowing for another level of input-specific neuromodulation. These results represent an important step toward better understanding the afferent landscape of the LC.

MATERIALS and METHODS

Ethical Approval

All methods were in accordance with the guidelines of and approved by the Institutional Animal Care and Use Committee (IACUC Approval #00155) at the University of Colorado Anschutz Medical Campus. For all experiments, heterozygous CaMKII α -Cre mice were used (Tsien et al., 1996). Animals were bred in house between homozygous CaMKII α -Cre (B6.Cg-Tg(Camk2a-cre)T29-1Stl/J; Jackson Labs, Stock No. 005359) and C57/BL6J (Jackson Labs, Stock No. 000664). Mice were maintained on a 12 hour light:dark cycle and were provided access to food and water ad libitum. Male and female mice were used for all experiments.

Stereotaxic Surgery

Mice underwent stereotaxic surgery between P25 and P35. Following anesthesia (1 – 2 % isoflurane) animals were placed on a stereotaxic apparatus (Kopf Instruments). Injections were performed at the following coordinates measured from bregma, LH: AP –.6 mm, ML +/- 1.2 mm, DV –5.3 mm; PAG: AP –3.15 mm, ML +/- 0.5 mm, DV –2.7 mm; PFC: AP +2.45 mm, ML +/- 0.5 mm, DV –1.8 mm. Using a Nanoject III (Drummond Scientific), either AAV-EF1a-doubled floxed-hChR2(H134R)-mCherry (AddGene 20297-AAV5) or AAV-EF1a-doubled floxed-hChR2(H134R)-EYFP (AddGene 20298-AAV5) was injected at a volume of 100 nL for LH, 50 nL for PAG, and 300 nL for PFC. As per nomenclature suggestions outlined in Laubach et al., 2018, injections to the medial prefrontal cortex specifically targeted the prelimbic and infralimbic cortices, with the target plane corresponding to 1.78 mm anterior from bregma in the mouse brain atlas (Franklin & Paxinos 3rd Edition, 2007). For simplicity, this afferent is referred to in the text as “PFC”. The volume of each injection site was optimized to the spread of the virus within that region, without spreading into neighboring regions. Mice received carprofen (5 mg/kg, subcutaneous) at the beginning of surgery and 24 hours post, after which they were monitored daily to ensure proper recovery.

Slice Preparation

Acute slices of the locus coeruleus were prepared at least 21 days after stereotaxic surgery (between P49 and P194). The mice were anesthetized with isoflurane and underwent cardiac perfusion with ice cold cutting solution (in mM: 75 NaCl, 2.5 KCl, 6 MgCl₂, 0.1 CaCl₂, 1.2 NaH₂PO₄, 25 NaHCO₃, 2.5 D-glucose, 50 sucrose; bubbled with 95% O₂ and 5% CO₂). The brains were then removed and placed on a VT1200 vibratome (Leica) where they were submerged in cutting solution that was continuously oxygenated (95% O₂, 5% CO₂) in a chamber surrounded by ice. For all animals, 240 μ m slices were collected from the LC as well as the site of injection (LH, PAG, or PFC); horizontal slices were obtained for the LC, LH, and PAG and the PFC was cut coronally. LC slices were transferred to a holding chamber containing oxygenated artificial cerebrospinal fluid (ACSF) containing in mM: 126 NaCl, 2.5 KCl, 1.2 MgCl₂, 2.5 CaCl₂, 1.2 NaH₂PO₄, 21.4 NaHCO₃, and 11.1 D-glucose; bubbled with 95% O₂ and 5% CO₂. Slices were allowed to recover for 1 hour in a water bath warmed to 32°C, where they remained until being transferred to the recording chamber for each experiment.

Slices obtained to verify the site of injection were moved to 4% paraformaldehyde immediately after they were collected and allowed to fix for 30 minutes at room temperature or overnight at 4°C. After fixation they were washed in PBS, mounted on a slide, and visualized (see imaging methods below). After visual inspection of the injection sites, animals were excluded if the center of the injection sat outside of the target area.

Electrophysiology

After at least one hour of recovery, electrophysiology experiments were recorded on LC slices. Slices were continuously perfused at 1.5 – 2 mL per minute with ACSF warmed to 30 ± 2°C. To isolate excitatory postsynaptic currents, picrotoxin (1 µM) was included in the bath for all experiments except for the case where the presence of potential GABA_A synaptic responses were being examined (shown in Fig 2). For dynorphin, CRF, oxytocin, and orexin A wash on experiments, the peptidase inhibitors bestatin (10 µM) and thiorphan (1 µM) were added to the ACSF with the peptide. Cells were visualized with a BX51WI microscope (Olympus) and the LC was identified as a cell body dense region between the corner of the 4th ventricle and the motor neurons of the mesencephalic tract; an unbiased approach was used to select cells throughout the LC, thus the recordings do not represent responses from any particular subregion. However, given the thickness of the slices, only 2–3 sections of the LC are able to be collected and most of the recordings represent the center of the LC within the DV axis. An AxoPatch 200B Amplifier (Molecular Devices) was used to collect recordings that were acquired with Axograph X (Axograph Scientific) at 5 kHz and filtered to 2 kHz. Pipettes were pulled from borosilicate glass (World Precision Instruments) using a PC-10 pipette puller (Narishige) and had a resistance around 1.5–2.0 MΩ. For cell attached experiments, the pipettes were filled with (in mM): 126 NaCl, 2.5 KCl, 1.2 MgCl₂, 2.5 CaCl₂, 1.2 NaH₂PO₄, 21.4 NaHCO₃, and 11.1 D-glucose. For whole cell recordings, KCl internal solution (135 mM KCl, 0.1 mM CaCl₂, 2 mM MgCl₂, 10 mM HEPES, 0.038 mM EGTA, 1 mg/ml ATP, 0.1 mg/ml GTP, 1.5 mg/ml phosphocreatine (pH 7.4, 275 mOsm)) was used for picrotoxin wash on experiments and Cesium Methanesulfonate internal solution (135 mM CsMeSulf, 0.1 mM CaCl₂, 2 mM MgCl₂, 10 mM HEPES, 0.1 mM EGTA, 6 mM TEA, 5 mM QX-314, 1 mg/ml ATP, 0.1 mg/ml GTP, 1.5 mg/ml phosphocreatine (pH 7.4, 275 mOsm)) was used for all other experiments. Cells were held at –60 mV for all whole cell experiments and recordings were excluded if a change in series resistance of more than 15 MΩ was detected. In a subset of cells, an electrically evoked (WPI Stimulus Isolator) α₂-mediated synaptic current (Egan et al., 1983) was used to confirm identity of LC-NE cells. For the cell fill experiments, biocytin was added to the internal solution (0.1%) and allowed to perfuse into the cell for at least 5 minutes. After careful removal of the patch pipette, the slices remained in the recording chamber for 10–20 minutes to allow residual biocytin to wash and slices were then transferred to 4% PFA.

Optogenetic stimulation was achieved using an LED (470 nm) through a 40x water immersion objective. Currents were evoked with wide-field stimulation using a 1-ms flash at a power at 0.8–1.0 mW/mm². Whole cell recordings used either a paired pulse (50 ms ISI) or a train of 5 pulses (50–400 ms ISI) and an intersweep interval of 30 seconds. Cell attached recordings used a train of 10 pulses (50 ms ISI) and an intersweep interval of 30 seconds.

Immunohistochemistry and Imaging

For verification of injection site, slices around the virally targeted region for each afferent type were collected and fixed as described above (slice preparation). The extent of viral expression and spread was visualized on a VS120 Slide Scanner (Olympus). No animals were included in the analysis that had off-target injections.

For visualization of biocytin-filled cells, slices were fixed in 4% PFA for 30 minutes at room temperature or overnight at 4°C. Slices were then incubated in streptavidin conjugated to Alexa-647 (1:500; ThermoFisher) and a tyrosine hydroxylase primary antibody (1:500; Millipore AB152), and then incubated in an Alexa488-conjugated secondary antibody (1:500; AbCam). Images were collected on a Zeiss LSM780.

For representative images of injection sites and terminal fields, a subset of mice that were not used for electrophysiology experiments underwent cardiac perfusion with 4% PFA. Brains were removed, incubated in 30% sucrose for at least 24 hours and rapidly frozen in embedding media (Richard Allan Scientific). Coronal sections (40 µm) were collected using a cryostat (Leica CM1950). Slices were immunostained for TH as above and the mCherry signal was amplified with Alexa-594 conjugated anti-mCherry (1:500; ThermoFisher). Images were collected on a Zeiss LSM780 and analyzed with ImageJ. Masks were drawn over the cell body region and the medial dendritic region according to the appearance of the TH signal. Within those regions, a mask was created within the mCherry channel using 2 standard deviations above the average mCherry signal of the image as a threshold. This mask was made binary and the raw integrated density within each masked region was divided by the area of that region to calculate the fractional density of the fibers.

Synaptophysin Labelling

Mice were injected as above with AAV-DIO-mGFP-2A-SyPhy-mRuby (Beier et al., 2015; Boxer et al., 2021). 240 µm horizontal sections of the LC were prepared as for electrophysiology experiments. As for the biocytin cell filling described above, LC-NE cells were targeted for whole cell recording with 0.1% biocytin in the patch pipette and ACSF as external solution. To allow for sufficient diffusion of biocytin to distal regions of the dendritic field, cells were held for 20 minutes. Pipettes were then gently removed from the cell surface and the slices went into 4% PFA for fixation after a 10–20 minute wash in ACSF. To increase visibility throughout their width, the slices were cleared with a CUBIC protocol. They were incubated in CUBIC Reagent 1 (in % w/v: 25 Urea, 25 Quadrol, 15 Triton X-100) at room temperature overnight, blocked in 0.5% fish gelatin (Sigma), immunostained with streptavidin conjugated to Alexa-647 (1:500; ThermoFisher), and incubated in CUBIC Reagent 2 (in % w/v: 25 Urea, 50 Sucrose, 10 Triethanolamine) overnight.

Images were collected on a Zeiss LSM780 and analyzed using ImageJ as follows. A 3D binary mask of the filled cell was generated manually using the Simple Neurite Tracer (SNT plugin for Fiji) with the default fill 'Distance Threshold'. To ensure that the cell soma was properly represented, a cylindrical region was manually defined and the cell mask within this region was dilated once using the Image J 3D Dilate function. A mask of the cell soma

could then be created by cropping the 3D cell fill mask to within the defined cylindrical region. A geodesic distance transform of the cell fill was generated using the MorphoLib toolbox (IJPB-plugins plugin for Fiji) Geodesic Distance function, with both the cell fill and soma masks as inputs. In the resulting distance image, each pixel represents the 3D distance along the cell fill to the soma. The MorphoLib function requires an equal XYZ pixel size so images were resized as needed without interpolation. Synaptophysin puncta were automatically identified by first applying a series of 2 filters to enhance punctate structure and signal; a 3D gaussian filter (sigma xyz = 1 px), followed by a 3D Laplacian filter (kernel xyz = [2 2 1] px) (MorphoLib 3D Filter). An intensity threshold was applied to the filtered image using the IsoData threshold on the full stack histogram with a light background to generate a puncta mask. This mask was visually inspected to confirm detected puncta matched the signal from the raw data; any clear instances of false puncta were manually deleted from the puncta mask. The resulting puncta mask was then multiplied by the cell fill mask (generated as described above) using an AND operation to include only regions co-localized to the cell fill. Cells were excluded from additional analysis if the maximum dendritic extension detected was less than 400 μm or if fewer than 15 overlapping puncta were detected (representing 1 standard deviation from the mean number of detected puncta). The 3D ROI toolbox (3D ImageJ Suite plugin for Fiji) was used to identify and label individual synaptophysin puncta. For each labeled puncta, two measurements were calculated using the 3D ROI toolbox. 1) The geodesic distance from the puncta to the cell soma. This was calculated using the 3D Intensity measure function with both the labeled synaptophysin puncta and the distance image (generated as described above) as inputs. 2) The surface area of the puncta, representing the contact surface area between synaptophysin and the cell. This was calculated using the 3D Geometrical Measure function, with the labeled puncta as input. Surface area measurements for each synaptophysin puncta were then binned based on their corresponding geodesic distance from the soma to generate a contact surface area profile. All Image J analysis macros available at https://github.com/mjkennedylab/Barcomb_et al2022

Chemicals

Picrotoxin (Tocris 1128), Tetrodotoxin (Tocris 1069), CRF (Tocris 1151), dynorphin A (Tocris 3195) OXA(17–33) (Tocris 5115), Oxytocin (Tocris 1910), Bestatin (Tocris 1956), and QX-314 (Tocris 2313) were obtained from Tocris. DL-Thiorphan (EMD-Millipore 598510) was obtained from Millipore. All other chemicals were from Sigma.

Statistical Analysis

All statistical analysis was performed with GraphPad Prism software. Data shown are all mean \pm SD in figures and mean \pm SD in text, with the exception of the time course data showing drug application that is presented in the upper panels of Figure 4 which illustrate mean \pm SEM. When applicable, parametric tests were used (paired t-test, one sample t-test, One-Way ANOVA/RMANOVA with post hoc Tukey's or Dunnett's test as applicable). Otherwise nonparametric analysis was used (Kruskal-Wallis ANOVA with post hoc Dunn's test). To compare distributions, a Komolgorov-Smirnov test was used. To calculate percent reduction after acute peptide wash on, data were normalized to control experiments with wash on of peptidase inhibitors alone, which resulted in a small run down

of EPSC amplitudes (10%). Statistical significance is denoted as */† $p < 0.05$, **/‡ $p < 0.01$, ***/ $p < 0.001$, and ns = not significant. Sample sizes are referred to by n/N = number of cells / number of animals.

Data Availability

All data are available upon request from the corresponding author (christopher.ford@cuanschutz.edu)

RESULTS

Anatomical distribution of isolated afferents within the LC

We first examined the pattern of expression of afferent inputs innervating the LC, by injecting CaMKII-Cre^{+/-} mice with AAV5-DIO-ChR2-mCherry into the lateral hypothalamus (LH), the lateral portion of the periaqueductal grey (PAG), or the medial prefrontal cortex (PFC). Injections resulted in a strong fluorescent signal at the injection site (Fig. 1A–C), which was verified for all animals.

Fluorescently labeled terminals from all three regions could be seen innervating the LC (Fig. 1D). Overall among groups we found that density of mCherry⁺ terminals innervating the LC was greatest from the LH, which was significantly greater than PAG (One-Way ANOVA, $F(2,20) = 4.31$, $p = 0.0277$, Post-Hoc Tukey's Test: LH > PAG, $p = 0.0394$) (Fig. 1E), suggesting that the LH may send a stronger input to the LC than the other two regions. Previous studies have noted sub-region differences in afferent distribution such that PFC and PAG afferents preferentially target the medial extension of the dendritic field with only sparse labelling within the cell body region (Arnsten and Goldman-Rakic, 1984; Ennis et al., 1991) whereas LH inputs display the opposite pattern, with a stronger innervation of the somatic region (Cedarbaum and Aghajanian, 1978). To examine this further, we compared the density of mCherry⁺ terminals along the anteroposterior (A/P) axis and between the somatic and dendritic fields. LH inputs varied across the A/P axis, with the lowest density of mCherry⁺ terminals found in the anterior end of the LC and the highest density in the posterior LC (One-Way ANOVA; $F(2,20) = 41.56$, $p < 0.0001$) (Fig. 1D, 1F & 1G). A similar density of LH inputs was found across somatic and dendritic areas. These results indicate that the LH preferentially targets the posterior zone of both LC somatic and dendritic regions. No differences were found with respect to PAG input density for either A/P axis or subcellular region, indicating that PAG inputs may equally target all areas of the LC (Fig 1D, 1F and 1G). Conversely, PFC inputs had stronger innervation of dendritic areas compared to the soma ($t = 6.84$, $p < 0.0001$) but did not vary across the A/P axis, suggesting that the PFC more selectively innervates dendritic portions of the LC but does so equally across the anteroposterior axis (Fig 1D, 1F & 1G). Thus while the LH has the highest density of afferents innervating the LC, each region exhibits differing patterns of innervation with the region.

While fluorescent afferents suggests that each region projects to the LC, mCherry-labeled axons may represent fibers of passage or synapses on to neighboring non-NE neurons, especially in the pericoerulear area medial to the LC. To further confirm the presence of

synapses onto LC-NE cells for each afferent, we injected an AAV encoding Cre-dependent mRuby-tagged synaptophysin (AAV-DIO-mGFP-2A-SyPhy-mRuby) (Beier et al., 2015; Boxer et al., 2021) into the LH, PFC or PAG of CaMKII-Cre^{+/-} mice. This method allows for the visualization of synaptic puncta from each afferent region. Individual LC-NE cells in horizontal slices were filled with biocytin and the slices were cleared using a CUBIC protocol (Fig. 1H). mRuby⁺ puncta overlapping with biocytin-filled LC-NE cells were identified and the number of puncta determined. Surprisingly, no significant difference was detected in the overall puncta density between afferents, though there was a trend toward the PFC having a lower density than the other two (Fig. 1I; One Way ANOVA, $F(2,24) = 2.73$, $p = 0.08$). We also examined the distribution of the puncta over the extent of the neurons, comparing somatic to dendritic regions (Fig. 1J). Segments of dendrites were analyzed in 100 μm bins and the surface area covered by mRuby⁺ puncta within that bin was measured (Fig. 1J) and the percent of puncta within each bin for the soma and first four distance segments was calculated (Fig. 1K). For both the LH and PAG, there was a similar proportion of puncta on the soma and the most proximal dendritic segment and a marked reduction across the segments farther than 200 μm from the soma (RMANOVA, LH: $F(2.8, 25.4) = 37.3$, $p < 0.0001$; PAG: $F(2.8, 19.5) = 32.9$, $p < 0.0001$). Though there was a significant difference between bins for PFC puncta, they more regularly distributed, with the proportion of puncta in the farthest distance bin not significantly different than the soma (RMANOVA, $F(2.6, 21.2) = 3.23$, $p = 0.048$).

Thus the PFC, LH and PAG all innervate LC-NE neurons, with the LH and PAG more heavily targeting proximal somatodendritic regions with the PFC displaying a broader distribution.

Glutamate afferents to the LC differ in their basal properties

While the above results, as well as previous tracing studies (Arnsten and Goldman-Rakic, 1984; Cameron et al., 1995; Cedarbaum and Aghajanian, 1978; Ennis et al., 1991; Hurley et al., 1991; Mantyh, 1983) suggest that the LH, PAG and PFC all innervate the LC, we reasoned that the strength and properties of synaptic inputs may vary among the different regions. To test this whole-cell voltage clamp recordings were made from LC neurons in slices from CaMKII-Cre^{+/-} mice injected with AAV-DIO-ChR2-mCherry (or eYFP) in either the LC, PAG or the PFC, and afferent terminals were optogenetically activated to evoke excitatory postsynaptic currents (EPSCs). LC-NE cells in horizontal slices were identified by their location in relation to the 4th ventricle, large soma size, and the presence of a characteristic α_2 -mediated IPSC (Courtney and Ford, 2014; Egan et al., 1983). In a subset of cells, we also included biocytin (0.1%) in the patch pipette and subsequently counter-stained the tissue for tyrosine hydroxylase (TH) to confirm post-hoc that recordings were made from TH⁺ neurons (Fig. 2A). Correct targeting of injection sites by fluorescence expression was verified in all mice.

In the presence of the GABA_A-receptor antagonist picrotoxin (100 μM), photo-activation of LH afferents (1 ms, 470 nm) elicited EPSCs in nearly all LC-NE cells (95%, 181/190 cells, N = 45 mice) (Fig. 2B). Optogenetic stimulation of PAG and PFC afferents also resulted in EPSCs in a majority of cells (PAG: 67%, 173/260 cells, N = 49 mice; PFC: 85%,

362/424 cells, $N = 82$ mice), however a lower proportion of LC-NE neurons were activated by these inputs ($\chi^2 = 67.80$, $p < 0.0001$) (Fig. 2B). Thus, afferents significantly differ with respect to connectivity within the LC such that a higher percentage of LC-NE cells receive LH input as compared to PFC and PAG, which is in line with the previous anatomical data that found a higher density of afferents innervating the LC from the LH compared to the other two regions. As expected, optically-evoked synaptic responses resulted from monosynaptic connections to LC-NE neurons as EPSCs driven by each input were abolished by tetrodotoxin (TTX; 1 μM) but restored by subsequent application of 4-aminopyridine (4-AP; 500 μM), which allows for presynaptic glutamate release while blocking axonal action potential propagation (Petreanu et al., 2009) (% baseline EPSC amplitude: LH: TTX = $15 \pm 5\%$, 4-AP = $139 \pm 27\%$, $n = 4$, $t = 8.40$, $**p = 0.0035$; PAG: TTX = $7 \pm 2\%$, 4-AP = $264 \pm 50\%$, $n = 4$, $t = 10.17$, $**p = 0.0020$; PFC: TTX = $18 \pm 22\%$, 4-AP = $272 \pm 203\%$, $n = 16$, $t = 5.11$, $***p = 0.0001$; paired t-test) (Fig. 2C–2D). To confirm that EPSCs were mediated by glutamate we repeated these experiments in the absence of synaptic blockers. For all three inputs, EPSCs were inhibited by the addition of the non-NMDA ionotropic glutamate receptor antagonist DNQX (10 μM) ([Baseline – DNQX]: LH: 108.0 ± 35.9 pA, paired $t = 6.73$, $p = 0.0013$, $n/N = 5/5$; PAG: 72.9 ± 48.0 pA, paired $t = 4.02$, $p = 0.0035$, $n/N = 7/6$; PFC: 39.9 ± 33.8 pA, paired $t = 2.36$, $p = 0.0496$, $n/N = 4/4$) but were unaffected by the GABA_A-receptor antagonist picrotoxin (100 μM) ([Baseline – Picro]: LH: 0.8 ± 4.4 pA, paired $t = 0.38$, $p = 0.36$, $n/N = 5/2$; PAG: 19.3 ± 59.0 pA, paired $t = 0.65$, $p = 0.28$, $n/N = 4/1$; PFC: 4.5 ± 8.5 pA, paired $t = 1.75$, $p = 0.06$, $n/N = 12/6$) (Fig. 2E–2F). Thus LH, PAG and the PFC form monosynaptic glutamatergic connections with LC-NE neurons.

Having shown that the three afferents form glutamatergic synapses onto LC-NE neurons, we next examined how inputs may differ in their basal synaptic properties. For this analysis, data were collected throughout the duration of the study and pooled in order to visualize the distribution for each parameter (LH: $n/N = 177/45$; PAG: $n/N = 165/49$; PFC: $n/N = 311/82$). We found that synaptic responses differed among inputs in regards to their basal amplitude, onset latency, and activation and decay kinetics (Fig. 2G–2J).

LH afferents on average evoked the largest amplitude EPSCs (145.8 ± 106.7 pA), followed by afferents from the PAG (83.0 ± 63.3 pA) and PFC (71.2 ± 70.6 pA) ($H(2) = 88.36$, $p < 0.0001$; LH vs. PAG $p < 0.0001$, LH vs. PFC $p < 0.0001$, PAG vs. PFC $p = 0.0244$; Kruskal-Wallis ANOVA with posthoc Dunn's test) (Fig. 2G, 2H). Thus, consistent with the higher density of LH fibers in the LC and greater proportion of LC-NE neurons showing LH-induced increases in excitability, LH afferents evoked the largest amplitude responses compared with the other two inputs.

To compare the kinetics of the synaptic events from each input, we measured the activation kinetics (10 – 90 % rise time) and decay kinetics (time constant of decay) following optogenetic stimulation of each set of afferents. Inputs from the PFC had faster activation kinetics (1.42 ± 0.77 ms) than those from the LH (2.06 ± 1.23 ms) or PAG inputs (1.98 ± 1.43 ms) (Kruskal Wallis $H(2) = 52.96$, $p < 0.0001$; Dunn's test, LH vs. PAG $p = 0.286$, LH vs. PFC $p < 0.0001$, PAG vs. PFC $p < 0.0001$) (Fig. 2G, 2I) while inputs from the LH evoked EPSCs with slower rates of decay (6.30 ± 2.45 ms) than those from the PAG (5.48

± 2.90 ms) or PFC (5.58 ± 3.23 ms) (Kruskal Wallis $H(2) = 22.54$, $p < 0.0001$; Dunn's test, LH vs. PAG $p = 0.0003$, LH vs. PFC $p < 0.0001$, PAG vs. PFC $p > 0.99$) (Fig. 2G, 2J).

In addition to making comparisons between inputs, all measures were compared between males and females. The LC is noted for its sexual dimorphism (Bangasser et al., 2016; Joshi and Chandler, 2020), including greater volume and dendritic complexity in females (Bangasser et al., 2011; Luque et al., 1992). Though a greater total number of inputs is observed in female mice, the density of innervation from the cortex, hypothalamus, and PAG specifically has not been found to not differ (Sun et al., 2020). There were no consistent differences across all inputs, though there were some subtle differences observed for PFC inputs in that the decay constant was longer in females (6.26 ± 4.04 ms) than males (5.05 ± 2.29 ms) (Mann-Whitney $U = 9830$, $p = 0.0140$). No differences in kinetics or basal amplitudes were observed for LH or PAG inputs. This lack of major differences between males and females is consistent with the observations of Sun et al. (2020).

Finally, we wanted to examine whether the activity of the glutamatergic inputs from the LH, PAG and PFC could drive phasic firing increases in LC cells. Firing rate was measured in cell attached recordings, which were followed by whole cell recordings to verify the presence of a synaptic response. Prior to stimulation, LC-NE cells had a characteristic pacemaker firing (0.54 ± 0.33 Hz; $n/N = 28/16$) (Fig. 2K–2M). Optogenetic stimulation (10 flashes, 20 Hz, 1 ms each) of LH terminals, PAG terminals, or PFC terminals all led to a phasic increase in the firing rate of LC-NE cells (LH inputs: 1.76 ± 0.71 Hz, $n/N = 7/6$; paired t-test, $t = 5.24$, $p = 0.0019$; PAG inputs: 1.43 ± 0.71 Hz, $n/N = 13/3$; paired t-test, $t = 4.36$, $p = 0.0009$; PFC inputs: 1.72 ± 0.81 Hz, $n/N = 8/7$; paired t-test, $t = 3.52$, $p = 0.0098$) (Fig. 2 K–2M). Thus, all three regions mediate an excitatory influence on LC-NE neuron activity that initiates a burst firing pattern.

Taken together, these observations support a model by which LH inputs are basally stronger and synapse close to the cell body. They also have a longer active time due to a slower decay. On the other hand, PFC inputs were rather weak with a short active time due to a fast onset and rise time. Inputs from the PAG had a notably long onset and were also weaker than those from the LH.

Glutamatergic afferents to the LC differ in release probability

We next examined how the probability of glutamate release varies among these inputs by measuring the paired-pulse ratios (PPRs) of EPSCs in LC-NE neurons during brief trains of stimulation. We first pooled data from recordings obtained throughout the study where inputs were stimulated with paired optogenetic stimuli with a 50 ms interstimulus interval (ISI) (LH: $n/N = 149/44$; PAG: $n/N = 130/50$; PFC: $n/N = 298/58$) (Fig. 3A–3B). PAG inputs differed from the other two regions, such that PAG-evoked EPSCs facilitated (PPR = 1.20 ± 0.51) whereas LH- and PFC-mediated EPSCs depressed (PPR = 0.71 ± 0.27 and 0.81 ± 0.50 , respectively) (Kruskal Wallis $H(2) = 80.11$, $p < 0.0001$; Dunn's test, LH vs. PAG $p < 0.0001$, LH vs. PFC $p = 0.874$, PAG vs. PFC $p < 0.0001$) (Fig. 3B). This suggests that inputs from the LH and PFC have a higher probability of release than those from the PAG. Throughout this data set we found that PPRs did not correlate with the amplitude of the initial oEPSC, indicating that observed differences in release probability (Pr) were

unlikely due to potential differences in the strength of input stimulation due to differences in channelrhodopsin expression (Fig. 3C).

Like the amplitude and kinetic measures, we also compared PPRs between males and females for all inputs. Of the three, only LH inputs displayed sexual dimorphic PPR values for the 50 ms ISI. On average, the PPR for females (0.77 ± 0.23 , $n = 82$) was greater than that for males (0.63 ± 0.30 , $n = 67$) ($t = 3.32$, $p = 0.0011$; data not shown).

In addition to comparing the single paired pulse response, a train of 5 pulses at a 50 ms ISI (20 Hz) was applied in a subset of cells. These data provide additional information related to release probability during repeated stimulation. For LH inputs, depression was present on each subsequent pulse to the first (Fig. 3D) (RMANOVA ($F(4,40) = 19.70$, $p < 0.0001$). The PAG responses facilitated on all pulses with no observed differences in ratios for any pulse (RMANOVA $F(4,28) = 1.83$, $p = 0.15$; Fig. 3E). The PFC responses were similar to LH responses such that depression was observed on all pulses (Fig. 3F) (RMANOVA, $F(4,56) = 2.72$, $p = 0.0383$).

As the extent of presynaptic facilitation and depression varies in a frequency-dependent manner, we next measured the PPRs in a subset of cells across a range of inter-stimulus intervals. While all three inputs varied across stimulation frequencies (LH: RMANOVA $F(4,40) = 5.93$, $p = 0.0008$; PAG: RMANOVA $F(4,28) = 2.95$, $p = 0.0376$; PFC: RMANOVA $F(4,60) = 5.60$, $p = 0.0007$), the pattern differed for LH and PFC inputs compared to PAG (Fig. 3G–3I). Low frequency stimulation led to a greater depression of EPSCs evoked from LH and PFC inputs (Fig. 3G, 3I), indicating that low frequency LH and PFC inputs are more preferentially filtered. In contrast, PAG inputs varied across ISIs with both low and high frequency stimulation evoking EPSCs that facilitated while moderate frequency stimulation (200 ms) evoked EPSCs that depressed (Fig. 3H).

Taken together, these results show that basal synaptic strength varies between inputs, with glutamatergic synapses created by PAG inputs having a comparatively lower initial release probability compared to the higher release probability of LH and PFC inputs. The high *Pr* of LH inputs, together with their denser innervation and larger amplitude of evoked EPSCs suggests that this input is a stronger excitatory input than inputs from the PAG and PFC.

CRF inhibits glutamate inputs from the PAG

CRF has an established role in increasing the activity of LC-NE neurons, especially during stress (Curtis et al., 1993, 1997; Imaki et al., 1993; McCall et al., 2015; Valentino et al., 1983). Though CRF may be acting directly on LC-NE neurons through postsynaptic CRF receptors (Reyes et al., 2006, 2008), there is also evidence for modulation of glutamatergic synapses. CRF release sites in the LC are found on presynaptic terminals apposed to glutamatergic synapses (Van Bockstaele et al., 1996) and a proportion of CRF receptors are presynaptic (Reyes et al., 2008). Induction of CRF release within the LC *in vivo* is sufficient to drive anxiety-like behavior (McCall et al., 2015) and acute stress led to a decrease in the amplitude of sEPSCs in rats (Borodovitsyna et al., 2018). Further, a previous study in rats found that acute application of CRF dose dependently induces a small but significant change in the amplitudes of spontaneous EPSCs (sEPSCs) (Prouty et al., 2017). Notably,

the relatively small magnitude of the change may be consistent with selective targeting of individual afferents rather than a large, global effect on all glutamatergic inputs.

To determine if modulation of the individual glutamatergic afferents occurs, we examined the effect of CRF on the isolated LH, PAG, and PFC inputs. EPSCs were again recorded from LC-NE neurons and 100 nM CRF was applied. While CRF had no effect on EPSCs evoked from LH or PFC inputs (LH: $97.00 \pm 17.33\%$, $t = 0.67$, $p = 0.513$; PFC: $106.1 \pm 19.84\%$, $t = 1.15$, $p = 0.272$), it did inhibit the amplitude of EPSCs evoked following stimulation of PAG terminals by $18.58 \pm 21.94\%$ (one sample t-test, $t = 3.05$, $p = 0.0100$) (Fig. 4A). Thus while CRF does not alter glutamate transmission from all terminals it inhibits inputs from the PAG.

OrexinA and Oxytocin do not strongly modulate selected glutamatergic synapses

The LC expresses high levels of the orexin 1 receptor (Ox1R) (Marcus et al., 2001; Trivedi et al., 1998). OrexinA (OxA) is a potent agonist of Ox1R and is synthesized within hypothalamic cells that send a very dense projection to the LC (de Lecea et al., 1998; Nambu et al., 1999; Peyron et al., 1998; Sakurai et al., 1998). Release of OxA within the LC has been linked to arousal (Bourgin et al., 2000; Carter et al., 2010; Gompf and Aston-Jones, 2008) and fear-dependent behavioral responses (Soya et al., 2017). OxA increases the firing of LC-NE neurons (Bourgin et al., 2000; Hagan et al., 1999; van den Pol et al., 2002) and increases glutamate release within the LC (Kodama and Kimura, 2002) however it is not known whether it selectively alters glutamatergic transmission of different inputs to the LC. To determine if OxA altered the strength of glutamate inputs from the LH, PAG and PFC, EPSCs were again recorded and the effect of OxA (1 μ M) examined following optogenetic stimulation of inputs from each region. Acute OxA (1 μ M) however had no effect on EPSCs evoked from any of the three regions (Fig. 4B) (LH: $99.93 \pm 14.71\%$, $t = 0.02$, $p = 0.985$; PAG $81.40 \pm 46.10\%$, $t = 1.46$, $p = 0.171$; PFC: $104.20 \pm 29.05\%$, $t = 0.52$, $p = 0.613$). Thus the excitatory effects of OxA found previously may result from other mechanisms or from alterations in the strength of other inputs not examined here.

Oxytocin (OT), and its associated receptor have been found within the LC (Hawthorn et al., 1984; Ostrowski, 1998; Rosen et al., 2008). Though it is commonly linked to social behavior, its role in the LC is not well understood. Because it decreases the firing rate of LC-NE neurons, it has been proposed to be anxiolytic. Conversely, it has also been shown to increase the frequency of sEPSCs (Wang et al., 2021). However like OxA, oxytocin however did not alter the amplitude of EPSCs originating from the PAG, LH or PFC (Fig. 4C) (LH: $100.30 \pm 18.53\%$, $t = 0.05$, $p = 0.960$; PAG $93.11 \pm 23.13\%$, $t = 1.11$, $p = 0.285$; PFC: $94.34 \pm 25.79\%$, $t = 0.79$, $p = 0.444$). This suggests that similar to OxA, effects of OT may result from modulation of inputs other than those from the PAG, LH or PFC.

Dynorphin inhibits glutamate inputs from the LH and PAG

Dynorphin is released in the LC at the succession of a stress response (Abercrombie and Jacobs, 1988; Kreibich et al., 2008). Kappa receptor activation has been shown to depress excitatory inputs in the LC (McFadzean et al., 1987) and endogenous dynorphin release depresses glutamate-dependent burst firing (Kreibich et al., 2008). Further, electron

microscopy studies have suggested that dynorphin release sites are present on putative excitatory synapses and have the potential to modulate glutamatergic release (Reyes et al., 2009, 2007), however it is not known whether dynorphin and kappa opioid receptor activation has differential effects on select inputs. We found that dynorphin (200 nM) reduced the amplitude of LH-evoked EPSCs by $51.5 \pm 15.19\%$ ($t = 13.99$, $p < 0.0001$, $n/N = 17/10$, one sample t-test) (Fig. 4D). Similarly, dynorphin reduced PAG-evoked EPSCs by $44.17 \pm 30.31\%$ ($t = 5.65$, $p < 0.0001$, $n/N = 15/10$) (Fig. 4D). Conversely, PFC inputs were much less sensitive to the effect of dynorphin (Fig. 4D). There was not a significant change in amplitude after dynorphin ($t = 1.89$, $p = 0.0784$, $n/N = 16/11$) and the percent reduction was $12.9 \pm 6.8\%$. This reduction was significantly less than that observed from LH and PAG inputs (One-Way ANOVA, $F(2,45) = 11.1$, $p = 0.0001$; Tukey's test: ****LH vs PFC, **PAG vs. PFC, LH vs. PAG ns) (Fig. 4D). This small effect of dynorphin on EPSCs evoked from PFC terminals however was not reversed by naloxone, suggesting either a non-selective effect of dynorphin on these inputs or a small amount of run-down in the amplitude of PFC-evoked EPSCs (Fig. 4D). Thus, PFC inputs are less sensitive to dynorphin treatment than PAG and LH inputs.

No differences existed between males and females for any peptide-dependent effects.

DISCUSSION

While glutamate release within the LC has long been known to be important for driving burst activity, the LC afferent landscape has largely been understudied. Here, we used a combined optogenetic and electrophysiological approach to classify three isolated excitatory afferents, comparing their basal properties and capacity for peptide-dependent neuromodulation. We confirmed the presence of functional glutamatergic synapses from LH, PAG, and PFC inputs onto LC-NE neurons and found that they differ with respect to (1) anatomical innervation of the LC, (2) basal properties of kinetics, connectivity, and release probability, and (3) extent of neuromodulation.

Anatomical innervation of the LC:

We found differences in the pattern of terminals within the area of the LC. For PFC afferents, previous studies have suggested afferents target the dendritic region medial to the LC, with only sparse labeling within the cell body region, and are more localized to the rostral extent of the LC (Arnsten and Goldman-Rakic, 1984; Hurley et al., 1991). Though we did not find a significant pattern along the rostrocaudal axis, PFC inputs did more densely innervate the dendritic region than the somatic region. Conversely, LH afferents strongly targeted the cell body region, which is consistent with previous results (Cedarbaum and Aghajanian, 1978). Interestingly, LH inputs also displayed a higher density in the posterior end of the LC, though the presence of fluorescence may represent fibers of passage rather than terminals. PAG inputs were not concentrated in any of the regions mentioned. Notably, prior tracing experiments related to the PAG afferent have found inconsistent results in the distribution of terminals and differential patterning dependent on the subregion of the PAG targeted (Bajic and Proudfit, 1999; Cameron et al., 1995; Ennis et al., 1991;

Mantyh, 1983). We focused on the ventrolateral PAG, as it has been shown to exert an excitatory influence within the LC (Ennis et al., 1991).

Because the medial extensions of LC dendrites intermingle with non-noradrenergic cells, including a population of pericoerulear inhibitory cells (Breton-Provencher and Sur, 2019), it has historically been difficult to distinguish afferents that synapse on distal dendrites with those on other cell types using traditional tracing techniques (Aston-Jones et al., 1986; Cedarbaum and Aghajanian, 1978; Schwarz et al., 2015). Importantly, we also used synaptophysin labeling to look for directly overlapping synaptic puncta with individual LC-NE neurons. This labelling showed a consistent distribution of puncta along the extent of LC-NE neurons for PFC afferents, in contrast with an increased concentration of puncta on the cell soma and proximal dendritic region from LH and PAG inputs.

Basal synaptic properties of afferents:

Surprisingly, the strongest afferent of the three in terms of connectivity and average response magnitude was the LH (Fig. 3–4). As the LH has not previously been appreciated as a major glutamatergic afferent to the LC, this result together with anatomical data suggests that it may play a significant role in regulating LC-NE neuron excitability. Various other differences in kinetics and paired pulse ratios may also be indicative of possible differences in presynaptic release machinery or postsynaptic receptor composition. In support of the LH being potential major excitatory input to the LC, we also found that this input along with PFC inputs to have a high release probability of glutamate release. Such specializations and functional consequences may be explored in more detail in future studies.

Peptidergic neuromodulation:

While OxA and OT had no effects on any of the inputs examined, both dynorphin and CRF had differential effects across inputs with dynorphin strongly inhibiting both LH and PAG inputs while CRF had modest but selective effects only on inputs from the PAG. These differences may be due the localization of receptors in the vicinity of the selected terminals. Dynorphin has long been known to regulate the LC and glutamate release onto these cells (Kreibich et al., 2008; McFadzean et al., 1987; Reyes et al., 2009, 2007) however it has not been clear which inputs, if any, it may selectively inhibit. The strength of inhibition however varied as both LH and PAG were strongly inhibited by dynorphin while there was no effect on inputs from the PFC. Past work has also found that CRF alters glutamatergic transmission (Prouty et al., 2017), matching anatomical work that has found CRF receptors on presynaptic afferents in the LC (Reyes et al., 2008). The distribution of these receptors and the strength of CRF to globally modulate glutamate inputs however has been unclear as spontaneous EPSCs are only slightly altered in the presence of CRF (Prouty et al., 2017). As we found that only PAG inputs were sensitive to CRF, the effect of CRF on spontaneous EPSCs may result from modulation of only selective inputs such as those originating from the PAG.

Peptide Interactions/Stress

While the present study examined the acute effects of dynorphin, OxA, OT and CRF, neuromodulation, the extent by which these peptides alter the strength of glutamatergic

inputs to the LC may be experience dependent, differing from that seen in naïve mice studied here. The magnitude of glutamate-dependent burst firing is known to change in response to behavioral manipulations such as binge eating (Bello et al., 2019) and alterations in glutamate receptor expression have been found in post mortem brains from human patients with depression (Bernard et al., 2011; Chandley et al., 2014; Davis et al., 2019). In addition to an apparent plasticity from the glutamate perspective, a number of changes in peptide receptor expression are induced by exposure to both acute and chronic stress. CRF receptor expression and sensitivity are upregulated (Curtis et al., 1999; Reyes et al., 2008, 2019), as is the expression of kORs (Lorca-Torralba et al., 2020). Similarly, the CRF-induced increase in tonic LC-NE firing rate becomes enhanced after stress (Jedema and Grace, 2003). If the surface expression of either CRF receptors or kORs changes on specific terminals, then the capacity for CRF and dynorphin modulation may likewise be unmasked.

There is also evidence for a change in OxA activity during opiate withdrawal, such that it displays a synergistic effect with glutamate on the firing rate of LC-NE neurons (Hooshmand et al., 2019). Further, OxA induces an atypical pattern of glutamatergic plasticity within the VTA such that it potentiates NMDAR responses in the short term while AMPAR responses potentiate 3 hours after OxA application (Borgland et al., 2006). Because the current study only considered the immediate, acute actions of OxA, a similar potential long term effect may be possible. This raises the possibility that OxA along with potentially the other peptides examined here may modulate LC glutamatergic synapses on either a longer time scale, target non-AMPA-dependent responses, or affect another subset of afferents, such as the paragigantocellular nucleus (Ennis et al., 1992).

Afferent Landscape

The results in this study confirm the presence of a monosynaptic glutamatergic connection from the PFC to the LC, and also suggest that the LH and PAG also form such connections. The LH in particular appears to be a strong input as it had the highest connectivity, basal amplitude, and initial release probability. The LH had been identified previously as the primary source of OxA to the LC, and a population of orexinergic afferents have been isolated previously (González et al., 2012; Sears et al., 2013; Soya et al., 2017). These prior studies targeted LH cells by the presence of OxA expression (Hcrt1+ cells), as opposed to the current strategy of isolating glutamatergic cells by the presence of CaMKII. Notably, the orexinergic terminals in the LC co-release glutamate (Henny et al., 2010; Sears et al., 2013) and have an asymmetric morphology, consistent with excitatory synapses (Horvath et al., 1999). There is additionally a third population of LC-projecting LH neurons that have been identified as GABAergic (Dimitrov et al., 2013). Whether these pathways overlap with the glutamatergic afferent isolated in the current study remains to be determined.

In addition to the afferents described here, it is likely that there are other glutamatergic afferents that have yet to be appreciated as many other LC afferents have not been fully explored. More studies such as this one comparing LC afferents are required to have a full understanding of the afferent landscape and how LC inputs contribute to the downstream effects of LC activation.

Of course, the field of GABAergic inputs to the LC is similarly understudied and further targeting of those afferents is also needed. Notably, a number of studies have focused on local GABAergic regulation of the LC from the pericoerulear region (Breton-Provencher and Sur, 2019; Gasparini et al., 2020; Kuo et al., 2020; Luskin et al., 2022). These neighboring cells intermingle with the dendritic region of the LC and display an inhibitory drive on LC-NE neurons. They also receive similar inputs as LC-NE neurons and future studies may consider the microcircuit effects of pericoerulear GABAergic neurons with LC-NE cells and their afferents. Inhibitory connections may also serve as a target of neuromodulation, in particular modulation of IPSCs by OxA has been noted previously (Kargar et al., 2018).

Afferent contributions to LC modularity

The LC is thought to be organized in modules defined by their projection target (Chandler et al., 2019; Plummer et al., 2020). An open question relates to whether there is input-output specificity within these modules. Most studies are consistent with a model of unbiased integration, such that afferents do not display a strong efferent-specific organization (Schwarz et al., 2015). Though this question was not explored in the current study, the high degree of connectivity, especially from LH inputs, is consistent with a lack efferent-specificity, at least for the three inputs examined here. Notably, an unbiased approach for cell selection was used, which did not permit for cell-type specific categorization of responders. Future studies may explore retro-labelling of efferent types or post-hoc immunostaining for markers of specific subtypes, such as galanin+ LC-NE neurons.

Though the current study does not provide evidence for or against input-output specificity, it does suggest that afferents display differing basal strengths and sensitivities to neuromodulation, which may confer a level of modularity. Because PFC afferents were insensitive to dynorphin-dependent depression, inputs from the PFC would be expected to maintain their basal level of strength during endogenous dynorphin release (e.g. offset of stress response). Conversely, LH and PAG inputs would decrease in strength.

Summary

The current results demonstrate the presence of multiple glutamatergic afferents to the LC that differ in their basal synaptic properties. These findings add to the body of evidence that the LC is not a homogeneous structure, but rather has a degree of heterogeneity that supports its role in a wide array of behaviors. An important caveat of the current study however is that some differences in ChR2-mediated evoked responses could be attributed to differences in viral uptake and expression). Further, it is possible that the viral spread either extends into neighboring regions that also project to the LC or does not fully encompass the projection within a particular subregion. Because the targeted regions are largely different in size (e.g. the PFC is much larger than the PAG) it is unlikely that the projections contained the same number of cells. Using more specific markers for each projection will be required to be able to allow for more complete targeting without the risk of significant spread into other potential afferents. However, the major takeaways of the current study are that monosynaptic glutamatergic connections exist between the targeted brain regions and that a subset of these synapses display differential sensitivity to neuromodulation. Future studies will be necessary

to probe the downstream consequences and network effects of these connections in order to provide a full picture of the input-output control of LC-NE neurons.

Supplementary Material

Refer to Web version on PubMed Central for supplementary material.

Acknowledgements:

We thank Jason Aoto for providing the AAV-DIO-mGFP-2A-SyPhy-mRuby and Radu Moldovan for use of the Zeiss LSM through the Advanced Light Microscopy Core at CU Anschutz.

Funding:

This work was funded by NIH grants R21-MH123085 (CPF and KB) R01-DA35821 (CPF), R01-NS95809 (CPF), NIMH F32-MH123053 (SSO), and NINDS R35-NS116879 (MJK).

Biography



Kelsey Barcomb joined Chris Ford's lab at the University of Colorado Anschutz Medical Campus in 2018. She obtained her PhD in pharmacology from the University of Colorado in 2015 and completed postdoctoral training with Julie Kauer at Brown University. Her research focuses on utilizing electrophysiology to study synaptic properties and plasticity.

Data availability statement:

All data reported in this paper will be shared by the lead contact upon request.

References

- Abercrombie ED, and Jacobs BL (1988). Systemic naloxone administration potentiates locus coeruleus noradrenergic neuronal activity under stressful but not non-stressful conditions. *Brain Res* 441, 362–366. 10.1016/0006-8993(88)91415-1. [PubMed: 3359238]
- Akaoka H, and Aston-Jones G (1991). Opiate withdrawal-induced hyperactivity of locus coeruleus neurons is substantially mediated by augmented excitatory amino acid input. *J. Neurosci* 11, 3830–3839. [PubMed: 1683899]
- Arnsten AF, and Goldman-Rakic PS (1984). Selective prefrontal cortical projections to the region of the locus coeruleus and raphe nuclei in the rhesus monkey. *Brain Res* 306, 9–18. 10.1016/0006-8993(84)90351-2. [PubMed: 6466989]
- Aston-Jones G, and Bloom FE (1981). Activity of norepinephrine-containing locus coeruleus neurons in behaving rats anticipates fluctuations in the sleep-waking cycle. *J. Neurosci* 1, 876–886. [PubMed: 7346592]
- Aston-Jones G, Ennis M, Pieribone VA, Nickell WT, and Shipley MT (1986). The brain nucleus locus coeruleus: restricted afferent control of a broad efferent network. *Science* 234, 734–737. [PubMed: 3775363]

- Aston-Jones G, Shipley MT, Chouvet G, Ennis M, van Bockstaele E, Pieribone V, Shiekhattar R, Akaoka H, Drolet G, and Astier B (1991). Afferent regulation of locus coeruleus neurons: anatomy, physiology and pharmacology. *Prog. Brain Res* 88, 47–75. 10.1016/S0079-6123(08)63799-1. [PubMed: 1687622]
- Bajic D, and Proudfit HK (1999). Projections of neurons in the periaqueductal gray to pontine and medullary catecholamine cell groups involved in the modulation of nociception. *J. Comp. Neurol* 405, 359–379. [PubMed: 10076931]
- Bangasser DA, Zhang X, Garachh V, Hanhauser E, and Valentino RJ (2011). Sexual dimorphism in locus coeruleus dendritic morphology: a structural basis for sex differences in emotional arousal. *Physiol. Behav* 103, 342–351. 10.1016/j.physbeh.2011.02.037. [PubMed: 21362438]
- Bangasser DA, Wiersielis KR, and Khantsis S (2016). Sex differences in the locus coeruleus-norepinephrine system and its regulation by stress. *Brain Res* 1641, 177–188. 10.1016/j.brainres.2015.11.021. [PubMed: 26607253]
- Beier KT, Steinberg EE, DeLoach KE, Xie S, Miyamichi K, Schwarz L, Gao XJ, Kremer EJ, Malenka RC, and Luo L (2015). Circuit Architecture of VTA Dopamine Neurons Revealed by Systematic Input-Output Mapping. *Cell* 162, 622–634. 10.1016/j.cell.2015.07.015. [PubMed: 26232228]
- Bello NT, Yeh C-Y, and James MH (2019). Reduced Sensory-Evoked Locus Coeruleus-Norepinephrine Neural Activity in Female Rats With a History of Dietary-Induced Binge Eating. *Front. Psychol* 10.
- Bernard R, Kerman IA, Thompson RC, Jones EG, Bunney WE, Barchas JD, Schatzberg AF, Myers RM, Akil H, and Watson SJ (2011). Altered expression of glutamate signaling, growth factor, and glia genes in the locus coeruleus of patients with major depression. *Mol. Psychiatry* 16, 634–646. 10.1038/mp.2010.44. [PubMed: 20386568]
- Berridge CW, and Waterhouse BD (2003). The locus coeruleus-noradrenergic system: modulation of behavioral state and state-dependent cognitive processes. *Brain Res. Brain Res. Rev* 42, 33–84. 10.1016/S0165-0173(03)00143-7. [PubMed: 12668290]
- Borgland SL, Taha SA, Sarti F, Fields HL, and Bonci A (2006). Orexin A in the VTA is critical for the induction of synaptic plasticity and behavioral sensitization to cocaine. *Neuron* 49, 589–601. 10.1016/j.neuron.2006.01.016. [PubMed: 16476667]
- Borodovitsyna O, Flamini MD, and Chandler DJ (2018). Acute Stress Persistently Alters Locus Coeruleus Function and Anxiety-like Behavior in Adolescent Rats. *Neuroscience* 373, 7–19. 10.1016/j.neuroscience.2018.01.020. [PubMed: 29341884]
- Bourgin P, Huitrón-Résendiz S, Spier AD, Fabre V, Morte B, Criado JR, Sutcliffe JG, Henriksen SJ, and de Lecea L (2000). Hypocretin-1 modulates rapid eye movement sleep through activation of locus coeruleus neurons. *J. Neurosci* 20, 7760–7765. [PubMed: 11027239]
- Boxer EE, Seng C, Lukacsovich D, Kim J, Schwartz S, Kennedy MJ, Földy C, and Aoto J (2021). Neurexin-3 defines synapse- and sex-dependent diversity of GABAergic inhibition in ventral subiculum. *Cell Rep* 37, 110098. 10.1016/j.celrep.2021.110098. [PubMed: 34879268]
- Breton-Provencher V, and Sur M (2019). Active control of arousal by a locus coeruleus GABAergic circuit. *Nat. Neurosci* 22, 218–228. 10.1038/s41593-018-0305-z. [PubMed: 30643295]
- Cameron AA, Khan IA, Westlund KN, and Willis WD (1995). The efferent projections of the periaqueductal gray in the rat: a Phaseolus vulgaris-leucoagglutinin study. II. Descending projections. *J. Comp. Neurol* 351, 585–601. 10.1002/cne.903510408. [PubMed: 7721985]
- Carter ME, Yizhar O, Chikahisa S, Nguyen H, Adamantidis A, Nishino S, Deisseroth K, and de Lecea L (2010). Tuning arousal with optogenetic modulation of locus coeruleus neurons. *Nat. Neurosci* 13, 1526–1533. 10.1038/nn.2682. [PubMed: 21037585]
- Carter ME, Brill J, Bonnavion P, Huguenard JR, Huerta R, and de Lecea L (2012). Mechanism for Hypocretin-mediated sleep-to-wake transitions. *Proc. Natl. Acad. Sci. U. S. A* 109, E2635–44. 10.1073/pnas.1202526109. [PubMed: 22955882]
- Cedarbaum JM, and Aghajanian GK (1978). Afferent projections to the rat locus coeruleus as determined by a retrograde tracing technique. *J. Comp. Neurol* 178, 1–16. 10.1002/cne.901780102. [PubMed: 632368]

- Chandler DJ, Jensen P, McCall JG, Pickering AE, Schwarz LA, and Totah NK (2019). Redefining noradrenergic neuromodulation of behavior: impacts of a modular locus coeruleus architecture. *J. Neurosci* 39, 8239–8249. 10.1523/JNEUROSCI.1164-19.2019. [PubMed: 31619493]
- Chandley MJ, Szebeni A, Szebeni K, Crawford JD, Stockmeier CA, Turecki G, Kostrzewa RM, and Ordway GA (2014). Elevated gene expression of glutamate receptors in noradrenergic neurons from the locus coeruleus in major depression. *Int. J. Neuropsychopharmacol* 17, 1569–1578. 10.1017/S1461145714000662. [PubMed: 24925192]
- Courtney NA, and Ford CP (2014). The timing of dopamine- and noradrenaline-mediated transmission reflects underlying differences in the extent of spillover and pooling. *J. Neurosci* 34, 7645–7656. 10.1523/JNEUROSCI.0166-14.2014. [PubMed: 24872568]
- Curtis AL, Drolet G, and Valentino RJ (1993). Hemodynamic stress activates locus coeruleus neurons of unanesthetized rats. *Brain Res. Bull* 31, 737–744. 10.1016/0361-9230(93)90150-A. [PubMed: 8518964]
- Curtis AL, Lechner SM, Pavcovich LA, and Valentino RJ (1997). Activation of the locus coeruleus noradrenergic system by intracoerulear microinfusion of corticotropin-releasing factor: effects on discharge rate, cortical norepinephrine levels and cortical electroencephalographic activity. *J. Pharmacol. Exp. Ther* 281, 163–172. [PubMed: 9103494]
- Curtis AL, Pavcovich LA, and Valentino RJ (1999). Long-term regulation of locus coeruleus sensitivity to corticotropin-releasing factor by swim stress. *J. Pharmacol. Exp. Ther* 289, 1211–1219. [PubMed: 10336508]
- Davis MT, Hillmer A, Holmes SE, Pietrzak RH, DellaGioia N, Nabulsi N, Matuskey D, Angarita GA, Carson RE, Krystal JH, et al. (2019). In vivo evidence for dysregulation of mGluR5 as a biomarker of suicidal ideation. *Proc. Natl. Acad. Sci* 116, 11490–11495. 10.1073/pnas.1818871116. [PubMed: 31085640]
- Dimitrov EL, Yanagawa Y, and Usdin TB (2013). Forebrain GABAergic projections to locus coeruleus in mouse. *J. Comp. Neurol* 521, 2373–2397. 10.1002/cne.23291. [PubMed: 23296594]
- Egan TM, Henderson G, North RA, and Williams JT (1983). Noradrenaline-mediated synaptic inhibition in rat locus coeruleus neurones. *J. Physiol* 345, 477–488. [PubMed: 6141289]
- Ennis M, and Aston-Jones G (1988). Activation of locus coeruleus from nucleus paragigantocellularis: a new excitatory amino acid pathway in brain. *J. Neurosci* 8, 3644–3657. [PubMed: 3193175]
- Ennis M, Behbehani M, Shipley MT, Van Bockstaele EJ, and Aston-Jones G (1991). Projections from the periaqueductal gray to the rostromedial pericoerulear region and nucleus locus coeruleus: anatomic and physiologic studies. *J. Comp. Neurol* 306, 480–494. 10.1002/cne.903060311. [PubMed: 1713927]
- Ennis M, Aston-Jones G, and Shiekhhattar R (1992). Activation of locus coeruleus neurons by nucleus paragigantocellularis or noxious sensory stimulation is mediated by intracoerulear excitatory amino acid neurotransmission. *Brain Res* 598, 185–195. 10.1016/0006-8993(92)90182-9. [PubMed: 1336704]
- Foote SL, Aston-Jones G, and Bloom FE (1980). Impulse activity of locus coeruleus neurons in awake rats and monkeys is a function of sensory stimulation and arousal. *Proc. Natl. Acad. Sci. U. S. A* 77, 3033–3037. [PubMed: 6771765]
- Foote SL, Berridge CW, Adams LM, and Pineda JA (1991). Electrophysiological evidence for the involvement of the locus coeruleus in alerting, orienting, and attending. *Prog. Brain Res* 88, 521–532. 10.1016/S0079-6123(08)63831-5. [PubMed: 1813932]
- Gasparini S, Resch JM, Gore AM, Peltekian L, and Geerling JC (2020). Pre-locus coeruleus neurons in rat and mouse. *Am. J. Physiol. Regul. Integr. Comp. Physiol* 10.1152/ajpregu.00261.2020.
- Godfrey N, and Borgland SL (2019). Diversity in the lateral hypothalamic input to the ventral tegmental area. *Neuropharmacology* 154, 4–12. 10.1016/j.neuropharm.2019.05.014. [PubMed: 31103620]
- Gompf HS, and Aston-Jones G (2008). Role of orexin input in the diurnal rhythm of locus coeruleus impulse activity. *Brain Res* 1224, 43–52. 10.1016/j.brainres.2008.05.060. [PubMed: 18614159]
- González JA, Jensen LT, Fugger L, and Burdakov D (2012). Convergent inputs from electrically and topographically distinct orexin cells to locus coeruleus and ventral tegmental area. *Eur. J. Neurosci* 35, 1426–1432. 10.1111/j.1460-9568.2012.08057.x. [PubMed: 22507526]

- Hagan JJ, Leslie RA, Patel S, Evans ML, Wattam TA, Holmes S, Benham CD, Taylor SG, Routledge C, Hemmati P, et al. (1999). Orexin A activates locus coeruleus cell firing and increases arousal in the rat. *Proc. Natl. Acad. Sci. U. S. A* 96, 10911–10916. [PubMed: 10485925]
- Hajós M, and Engberg G (1990). A role of excitatory amino acids in the activation of locus coeruleus neurons following cutaneous thermal stimuli. *Brain Res* 521, 325–328. 10.1016/0006-8993(90)91560-4. [PubMed: 2169960]
- Hawthorn J, Ang VT, and Jenkins JS (1984). Comparison of the distribution of oxytocin and vasopressin in the rat brain. *Brain Res* 307, 289–294. 10.1016/0006-8993(84)90482-7. [PubMed: 6466998]
- Henny P, Brischoux F, Mainville L, Stroh T, and Jones BE (2010). Immunohistochemical evidence for synaptic release of glutamate from orexin terminals in the locus coeruleus. *Neuroscience* 169, 1150–1157. 10.1016/j.neuroscience.2010.06.003. [PubMed: 20540992]
- Hooshmand B, Azizi H, Ahmadi-Soleimani SM, and Semnani S (2019). Synergistic effect of orexin-glutamate co-administration on spontaneous discharge rate of locus coeruleus neurons in morphine-dependent rats. *Neurosci. Lett* 706, 12–17. 10.1016/j.neulet.2019.04.060. [PubMed: 31051222]
- Horvath TL, Peyron C, Diano S, Ivanov A, Aston-Jones G, Kilduff TS, and van Den Pol AN (1999). Hypocretin (orexin) activation and synaptic innervation of the locus coeruleus noradrenergic system. *J. Comp. Neurol* 415, 145–159. [PubMed: 10545156]
- Hurley KM, Herbert H, Moga MM, and Saper CB (1991). Efferent projections of the infralimbic cortex of the rat. *J. Comp. Neurol* 308, 249–276. 10.1002/cne.903080210. [PubMed: 1716270]
- Imaki T, Shibasaki T, Hotta M, and Demura H (1993). Intracerebroventricular administration of corticotropin-releasing factor induces *c-fos* mRNA expression in brain regions related to stress responses: comparison with pattern of *c-fos* mRNA induction after stress. *Brain Res* 616, 114–125. 10.1016/0006-8993(93)90199-W. [PubMed: 8358602]
- Jedema HP, and Grace AA (2003). Chronic exposure to cold stress alters electrophysiological properties of locus coeruleus neurons recorded in vitro. *Neuropsychopharmacology* 28, 63–72. 10.1038/sj.npp.1300020. [PubMed: 12496941]
- Jodo E, and Aston-Jones G (1997). Activation of locus coeruleus by prefrontal cortex is mediated by excitatory amino acid inputs. *Brain Res* 768, 327–332. 10.1016/S0006-8993(97)00703-8. [PubMed: 9369332]
- Jones BE, and Moore RY (1977). Ascending projections of the locus coeruleus in the rat. II. Autoradiographic study. *Brain Res* 127, 25–53. 10.1016/0006-8993(77)90378-X. [PubMed: 301051]
- Joshi N, and Chandler D (2020). Chapter 10 - Sex and the noradrenergic system. In *Handbook of Clinical Neurology*, Lanzenberger R, Kranz GS, and Savic I, eds. (Elsevier), pp. 167–176.
- Kargar HM-P, Azizi H, Mirnajafi-Zadeh J, Mani AR, and Semnani S (2018). Orexin A presynaptically decreases inhibitory synaptic transmission in rat locus coeruleus neurons. *Neurosci. Lett* 683, 89–93. 10.1016/j.neulet.2018.06.022. [PubMed: 29908258]
- Kodama T, and Kimura M (2002). Arousal effects of orexin-A correlate with GLU release from the locus coeruleus in rats. *Peptides* 23, 1673–1681. [PubMed: 12217428]
- Kreibich A, Reyes BAS, Curtis AL, Ecke L, Chavkin C, Van Bockstaele EJ, and Valentino RJ (2008). Presynaptic inhibition of diverse afferents to the locus coeruleus by kappa-opiate receptors: a novel mechanism for regulating the central norepinephrine system. *J. Neurosci* 28, 6516–6525. 10.1523/JNEUROSCI.0390-08.2008. [PubMed: 18562623]
- Kuo C-C, Hsieh J-C, Tsai H-C, Kuo Y-S, Yau H-J, Chen C-C, Chen R-F, Yang H-W, and Min M-Y (2020). Inhibitory interneurons regulate phasic activity of noradrenergic neurons in the mouse locus coeruleus and functional implications. *J. Physiol* 598, 4003–4029. 10.1113/JP279557. [PubMed: 32598024]
- Laubach M, Amarante LM, Swanson K, and White SR (2018). What, If Anything, Is Rodent Prefrontal Cortex? *ENeuro* 5. 10.1523/ENEURO.0315-18.2018.
- de Lecea L, Kilduff TS, Peyron C, Gao X, Foye PE, Danielson PE, Fukuhara C, Battenberg EL, Gautvik VT, Bartlett FS, et al. (1998). The hypocretins: hypothalamus-specific peptides with neuroexcitatory activity. *Proc. Natl. Acad. Sci. U. S. A* 95, 322–327. [PubMed: 9419374]

- Llorca-Torralba M, Pilar-Cuellar F, da Silva Borges G, Mico JA, and Berrocoso E (2020). Opioid receptors mRNAs expression and opioids agonist-dependent G-protein activation in the rat brain following neuropathy. *Prog. Neuropsychopharmacol. Biol. Psychiatry* 99, 109857. 10.1016/j.pnpbp.2019.109857. [PubMed: 31904442]
- Lopes LT, Patrone LGA, Li K-Y, Imber AN, Graham CD, Gargaglioni LH, and Putnam RW (2016). Anatomical and functional connections between the locus coeruleus and the nucleus tractus solitarius in neonatal rats. *Neuroscience* 324, 446–468. 10.1016/j.neuroscience.2016.03.036. [PubMed: 27001176]
- Luppi PH, Aston-Jones G, Akaoka H, Chouvet G, and Jouvet M (1995). Afferent projections to the rat locus coeruleus demonstrated by retrograde and anterograde tracing with cholera-toxin B subunit and Phaseolus vulgaris leucoagglutinin. *Neuroscience* 65, 119–160. 10.1016/0306-4522(94)00481-J. [PubMed: 7753394]
- Luque JM, de Blas MR, Segovia S, and Guillamón A (1992). Sexual dimorphism of the dopamine-beta-hydroxylase-immunoreactive neurons in the rat locus ceruleus. *Brain Res. Dev. Brain Res* 67, 211–215. [PubMed: 1511516]
- Luskin AT, Li L, Fu X, Barcomb K, Blackburn T, Li EM, Rana A, Simon RC, Sun L, Murry AD, et al. (2022). A diverse network of pericoerulear neurons control arousal states (*Neuroscience*).
- Mantyh PW (1983). Connections of midbrain periaqueductal gray in the monkey. II. Descending efferent projections. *J. Neurophysiol* 49, 582–594. 10.1152/jn.1983.49.3.582. [PubMed: 6300351]
- Marcus JN, Aschkenasi CJ, Lee CE, Chemelli RM, Saper CB, Yanagisawa M, and Elmquist JK (2001). Differential expression of orexin receptors 1 and 2 in the rat brain. *J. Comp. Neurol* 435, 6–25. 10.1002/cne.1190. [PubMed: 11370008]
- McCall JG, Al-Hasani R, Siuda ER, Hong DY, Norris AJ, Ford CP, and Bruchas MR (2015). CRH Engagement of the Locus Coeruleus Noradrenergic System Mediates Stress-Induced Anxiety. *Neuron* 87, 605–620. 10.1016/j.neuron.2015.07.002. [PubMed: 26212712]
- McFadzean I, Lacey MG, Hill RG, and Henderson G (1987). Kappa opioid receptor activation depresses excitatory synaptic input to rat locus coeruleus neurons in vitro. *Neuroscience* 20, 231–239. 10.1016/0306-4522(87)90015-7. [PubMed: 3031541]
- Nambu T, Sakurai T, Mizukami K, Hosoya Y, Yanagisawa M, and Goto K (1999). Distribution of orexin neurons in the adult rat brain. *Brain Res* 827, 243–260. 10.1016/S0006-8993(99)01336-0. [PubMed: 10320718]
- Ostrowski NL (1998). Oxytocin receptor mRNA expression in rat brain: implications for behavioral integration and reproductive success. *Psychoneuroendocrinology* 23, 989–1004. 10.1016/S0306-4530(98)00070-5. [PubMed: 9924748]
- Page ME, Akaoka H, Aston-Jones G, and Valentino RJ (1992). Bladder distention activates noradrenergic locus coeruleus neurons by an excitatory amino acid mechanism. *Neuroscience* 51, 555–563. 10.1016/0306-4522(92)90295-d. [PubMed: 1336819]
- Petersson M, Uvnäs-Moberg K, Erhardt S, and Engberg G (1998). Oxytocin increases locus coeruleus alpha 2-adrenoreceptor responsiveness in rats. *Neurosci. Lett* 255, 115–118. 10.1016/S0304-3940(98)00729-0. [PubMed: 9835228]
- Peyron C, Tighe DK, van den Pol AN, de Lecea L, Heller HC, Sutcliffe JG, and Kilduff TS (1998). Neurons containing hypocretin (orexin) project to multiple neuronal systems. *J. Neurosci* 18, 9996–10015. [PubMed: 9822755]
- Plummer NW, Chandler DJ, Powell JM, Scappini EL, Waterhouse BD, and Jensen P (2020). An Intersectional Viral-Genetic Method for Fluorescent Tracing of Axon Collaterals Reveals Details of Noradrenergic Locus Coeruleus Structure. *ENeuro* 7. 10.1523/ENEURO.0010-20.2020.
- van den Pol AN, Ghosh PK, Liu R-J, Li Y, Aghajanian GK, and Gao X-B (2002). Hypocretin (orexin) enhances neuron activity and cell synchrony in developing mouse GFP-expressing locus coeruleus. *J. Physiol* 541, 169–185. 10.1113/jphysiol.2002.017426. [PubMed: 12015428]
- Poller WC, Madai VI, Bernard R, Laube G, and Veh RW (2013). A glutamatergic projection from the lateral hypothalamus targets VTA-projecting neurons in the lateral habenula of the rat. *Brain Res* 1507, 45–60. 10.1016/j.brainres.2013.01.029. [PubMed: 23348378]

- Prouty EW, Waterhouse BD, and Chandler DJ (2017). Corticotropin releasing factor dose-dependently modulates excitatory synaptic transmission in the noradrenergic nucleus locus coeruleus. *Eur. J. Neurosci* 45, 712–722. 10.1111/ejn.13501. [PubMed: 27973694]
- Reyes B. a. S., Chavkin C, and van Bockstaele EJ (2009). Subcellular targeting of kappa-opioid receptors in the rat nucleus locus coeruleus. *J. Comp. Neurol* 512, 419–431. 10.1002/cne.21880. [PubMed: 19009591]
- Reyes BAS, Fox K, Valentino RJ, and Van Bockstaele EJ (2006). Agonist-induced internalization of corticotropin-releasing factor receptors in noradrenergic neurons of the rat locus coeruleus. *Eur. J. Neurosci* 23, 2991–2998. 10.1111/j.1460-9568.2006.04820.x. [PubMed: 16819988]
- Reyes BAS, Johnson AD, Glaser JD, Commons KG, and Van Bockstaele EJ (2007). Dynorphin-containing axons directly innervate noradrenergic neurons in the rat nucleus locus coeruleus. *Neuroscience* 145, 1077–1086. 10.1016/j.neuroscience.2006.12.056. [PubMed: 17289275]
- Reyes BAS, Valentino RJ, and Van Bockstaele EJ (2008). Stress-induced intracellular trafficking of corticotropin-releasing factor receptors in rat locus coeruleus neurons. *Endocrinology* 149, 122–130. 10.1210/en.2007-0705. [PubMed: 17947354]
- Reyes BAS, Zhang X-Y, Dufourt EC, Bhatnagar S, Valentino RJ, and Van Bockstaele EJ (2019). Neurochemically distinct circuitry regulates locus coeruleus activity during female social stress depending on coping style. *Brain Struct. Funct* 224, 1429–1446. 10.1007/s00429-019-01837-5. [PubMed: 30767070]
- Rosen GJ, de Vries GJ, Goldman SL, Goldman BD, and Forger NG (2008). Distribution of oxytocin in the brain of a eusocial rodent. *Neuroscience* 155, 809–817. 10.1016/j.neuroscience.2008.05.039. [PubMed: 18582538]
- Sakurai T, Amemiya A, Ishii M, Matsuzaki I, Chemelli RM, Tanaka H, Williams SC, Richardson JA, Kozlowski GP, Wilson S, et al. (1998). Orexins and Orexin Receptors: A Family of Hypothalamic Neuropeptides and G Protein-Coupled Receptors that Regulate Feeding Behavior. *Cell* 92, 573–585. 10.1016/S0092-8674(00)80949-6. [PubMed: 9491897]
- Sara SJ (2009). The locus coeruleus and noradrenergic modulation of cognition. *Nat. Rev. Neurosci* 10, 211–223. 10.1038/nrn2573. [PubMed: 19190638]
- Schwarz LA, Miyamichi K, Gao XJ, Beier KT, Weissbourd B, DeLoach KE, Ren J, Ibanes S, Malenka RC, Kremer EJ, et al. (2015). Viral-genetic tracing of the input-output organization of a central noradrenaline circuit. *Nature* 524, 88–92. 10.1038/nature14600. [PubMed: 26131933]
- Sears RM, Fink AE, Wiggestrand MB, Farb CR, de Lecea L, and Ledoux JE (2013). Orexin/hypocretin system modulates amygdala-dependent threat learning through the locus coeruleus. *Proc. Natl. Acad. Sci. U. S. A* 110, 20260–20265. 10.1073/pnas.1320325110. [PubMed: 24277819]
- Soya S, Takahashi TM, McHugh TJ, Maejima T, Herlitze S, Abe M, Sakimura K, and Sakurai T (2017). Orexin modulates behavioral fear expression through the locus coeruleus. *Nat. Commun* 8, 1606. 10.1038/s41467-017-01782-z. [PubMed: 29151577]
- Sun P, Wang J, Zhang M, Duan X, Wei Y, Xu F, Ma Y, and Zhang Y-H (2020). Sex-Related Differential Whole-Brain Input Atlas of Locus Coeruleus Noradrenaline Neurons. *Front. Neural Circuits* 14, 53. 10.3389/fncir.2020.00053. [PubMed: 33071759]
- Trivedi P, Yu H, MacNeil DJ, der Ploeg LHTV, and Guan X-M (1998). Distribution of orexin receptor mRNA in the rat brain. *FEBS Lett* 438, 71–75. 10.1016/S0014-5793(98)01266-6. [PubMed: 9821961]
- Tsien JZ, Chen DF, Gerber D, Tom C, Mercer EH, Anderson DJ, Mayford M, Kandel ER, and Tonegawa S (1996). Subregion- and cell type-restricted gene knockout in mouse brain. *Cell* 87, 1317–1326. 10.1016/s0092-8674(00)81826-7. [PubMed: 8980237]
- Valentino RJ, Foote SL, and Aston-Jones G (1983). Corticotropin-releasing factor activates noradrenergic neurons of the locus coeruleus. *Brain Res* 270, 363–367. [PubMed: 6603889]
- Van Bockstaele EJ, and Valentino RJ (2013). Neuropeptide regulation of the locus coeruleus and opiate-induced plasticity of stress responses. *Adv. Pharmacol* 68, 405–420. 10.1016/B978-0-12-411512-5.00019-1. [PubMed: 24054155]
- Van Bockstaele EJ, Colago EE, and Valentino RJ (1996). Corticotropin-releasing factor-containing axon terminals synapse onto catecholamine dendrites and may presynaptically modulate other afferents in the rostral pole of the nucleus locus coeruleus in the rat brain. *J. Comp. Neurol* 364,

523–534. 10.1002/(SICI)1096-9861(19960115)364:3<523::AID-CNE10>3.0.CO;2-Q. [PubMed: 8820881]

Wang X, Escobar JB, and Mendelowitz D (2021). Sex Differences in the Hypothalamic Oxytocin Pathway to Locus Coeruleus and Augmented Attention with Chemogenetic Activation of Hypothalamic Oxytocin Neurons. *Int. J. Mol. Sci* 22. 10.3390/ijms22168510.

Zitnik GA (2016). Control of arousal through neuropeptide afferents of the locus coeruleus. *Brain Res* 1641, 338–350. 10.1016/j.brainres.2015.12.010. [PubMed: 26688115]

Author Manuscript

Author Manuscript

Author Manuscript

Author Manuscript

Key Points Summary:

- Excitatory inputs to the locus coeruleus (LC) are important for driving norepinephrine neuron activity and downstream behaviors in response to salient stimuli, but little is known about the functional properties of different glutamate inputs that innervate these neurons
- We used a viral-mediated optogenetic approach to compare glutamate afferents from the prefrontal cortex (PFC), the lateral hypothalamus (LH) and the periaqueductal grey (PAG).
- While PFC was predicted to make synaptic inputs, we found that the LH and PAG also drove robust excitatory events in LC norepinephrine neurons.
- The strength, kinetics and short-term plasticity of each input differed as did the extent of neuromodulation by both dynorphin and corticotrophin releasing factor.
- Thus each input in displayed a unique set of basal properties and modulation by peptides. This characterization is an important step in deciphering the heterogeneity of the LC.

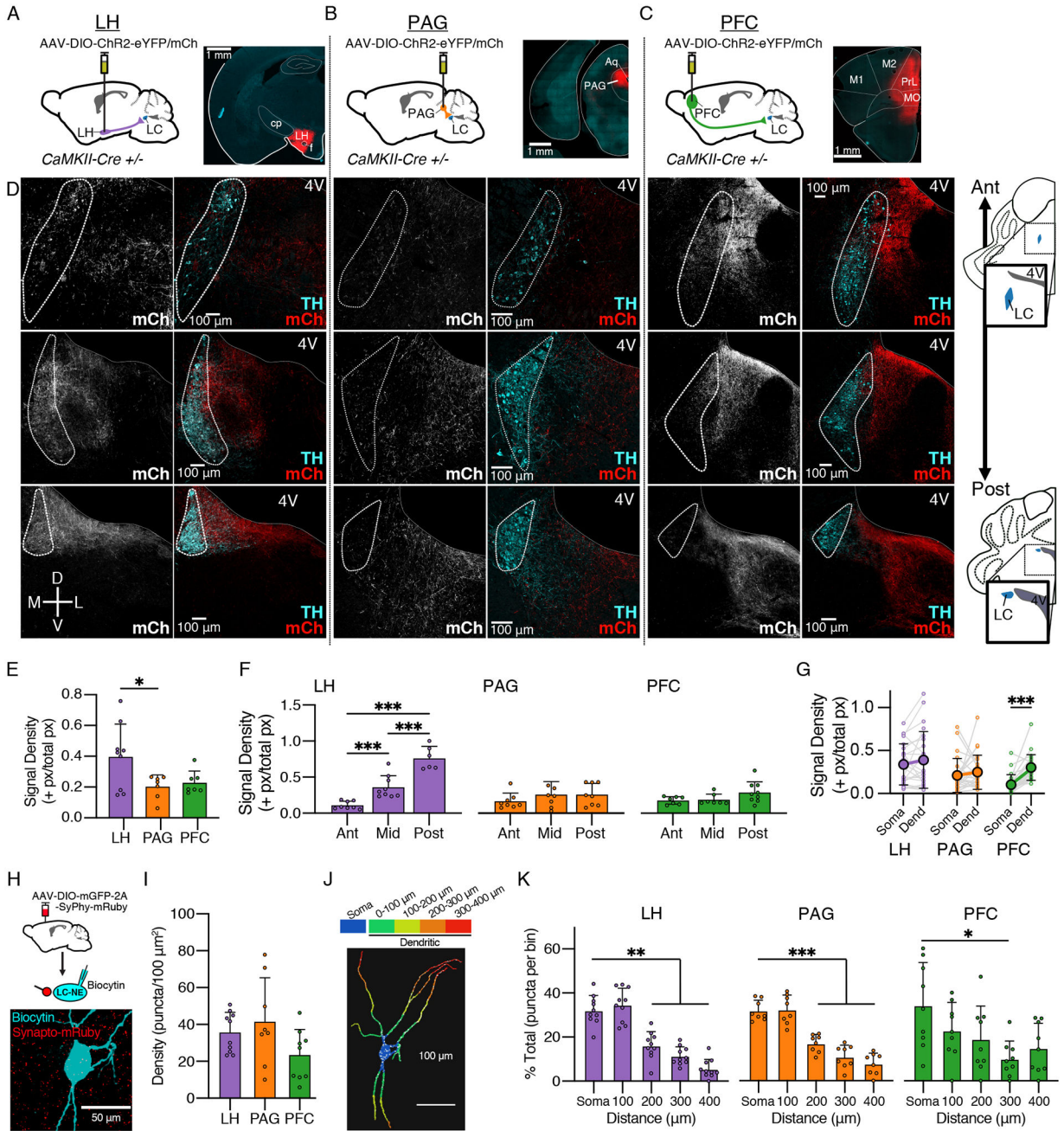


Figure 1. Differential targeting of glutamnergic inputs from the LH, PAG, and PFC to LC neurons. (A-C) Schematics of viral expression. AAV5-DIO-ChR2-eYFP/mCherry was injected into target sites in CaMKII-Cre^{+/-} mice. Representative images of injection sites are shown for each region. Targeted regions consisted of (A) lateral hypothalamus (LH), (B) lateral periaqueductal grey (PAG), and (C) medial prefrontal cortex (PFC) (*cp* = caudate putamen, *Aq* = aqueduct, *M1/M2* = motor cortices, *PrL* = prelimbic cortex, *MO* = motor orbital cortex). (D) Representative images of terminal fields of LH (left), PAG (center), and PFC (right) afferents within the LC at anterior (“ant”; top), mid-anteroposterior (middle row), and posterior (bottom) sections. Scale bars = 100 μm. Orientation: Ant = anterior, Post = posterior, D = dorsal, V = ventral, M = medial, L = lateral. (E) Signal density (+ px/total px) for LH, PAG, and PFC. LH shows significantly higher density than PAG and PFC (*). Error bars represent SEM. (F) Signal density (+ px/total px) for LH, PAG, and PFC at anterior (Ant), mid (Mid), and posterior (Post) sections. LH shows significantly higher density in all sections (***). Error bars represent SEM. (G) Signal density (+ px/total px) for LH, PAG, and PFC at somatic (Soma) and dendritic (Dend) compartments. LH shows significantly higher density in dendrites (***). Error bars represent SEM. (H) Schematic of viral expression (AAV-DIO-mGFP-2A-SyPhy-mRuby) and biocytin injection into the LC-NE. Representative image shows biocytin (blue) and synapto-mRuby (red) staining. Scale bar = 50 μm. (I) Density (puncta/100 μm²) for LH, PAG, and PFC. LH shows significantly higher density than PAG and PFC (***). Error bars represent SEM. (J) Color-coded dendritic field of a neuron. Soma size ranges: 0-100 μm (blue), 100-200 μm (green), 200-300 μm (yellow), 300-400 μm (red). Scale bar = 100 μm. (K) % Total (puncta per bin) for LH, PAG, and PFC at distances of 100, 200, 300, and 400 μm. LH shows significantly higher density at 100 and 200 μm (**). Error bars represent SEM.

posterior (“post”; bottom) sections. Gray/red channels show mCh corresponding to viral expression, green channel shows immunostain for TH. (*4V = fourth ventricle*)

(E) Quantification of the signal density for mCh expressing terminals at the locus coeruleus. The LH afferents (0.40 ± 0.21 +px/px, $N = 9$) had a higher density than those from the PAG (0.20 ± 0.08 +px/px, $N = 7$); PFC afferents did not significantly differ (0.23 ± 0.07 +px/px, $N = 7$) (One-Way ANOVA, $F(2,20) = 4.31$, $p = 0.0277$, post hoc Tukey’s test). $N =$ injected hemispheres.

(F) Quantification of the signal density for mCh expressing terminals at 3 anteroposterior (A/P) levels. The density of LH afferents (E) was lowest at the anterior and highest end of the LC (One-Way ANOVA, $F(2,22) = 31.77$, $p < 0.0001$, post hoc Tukey’s test). PAG afferents (F) and PFC afferents (G) did not display a significant pattern along the A/P axis. $n =$ images analyzed.

(G) Quantification of the signal density for mCherry⁺ terminals between the somatic region (TH⁺ cell bodies) and the dendritic region (medially extending TH⁺ signal). For PFC inputs ($n/N = 24/5$), the dendritic region had a greater signal density than the somal (paired t-test, $t = 6.84$, $p < 0.0001$). $n/N =$ images analyzed/mice.

(H) CaMKII-Cre^{+/-} mice were injected with AAV-DIO-mGFP-2A-SyPhy-mRuby into LH, PAG, or PFC. Representative image (from LH-injected animal) shows overlap between mRuby⁺ synaptophysin puncta with a biocytin filled LC-NE cell, labelled with Alexa-647 conjugated streptavidin.

(I) Quantification of puncta density, measured by number of puncta per $100 \mu\text{m}^2$ cell surface area. No difference was found between LH ($n/N = 10/3$), PAG ($n/N = 8/5$), or PFC ($n/N = 9/4$) terminals (One Way ANOVA, $F(2,23) = 2.42$, $p = 0.11$).

(J) 3D reconstruction of a cell fill, displaying distance bins used for analysis; overlapping puncta shown in white. Puncta within the somal region (blue) were compared to those in the dendritic region, which was binned in $100 \mu\text{m}$ increments.

(K) Quantification of puncta area within each distance bin. mRuby⁺ terminals were more concentrated in the soma than the dendrites past $100 \mu\text{m}$ from the edge of the soma for afferents from LH (Left; RMANOVA, $F(2.82,25.35) = 37.32$, $p < 0.0001$; post-hoc Dunnett’s test comparing each bin to soma) and PAG (Center; RMANOVA, $F(2.79,19.51) = 32.87$, $p < 0.0001$; post-hoc Dunnett’s test comparing each bin to soma). Distance from soma was also a significant factor in the distribution of puncta for PFC afferents, though only for a more distal section of the LC dendrites at $300 \mu\text{m}$ from the edge of the soma (Right; RMANOVA, $F(2.64,21.15) = 3.23$, $p = 0.0480$). $n =$ filled LC cells.

Summary data are mean \pm SD. * = $p < 0.05$, ** = $p < 0.01$, *** = $p < 0.001$.

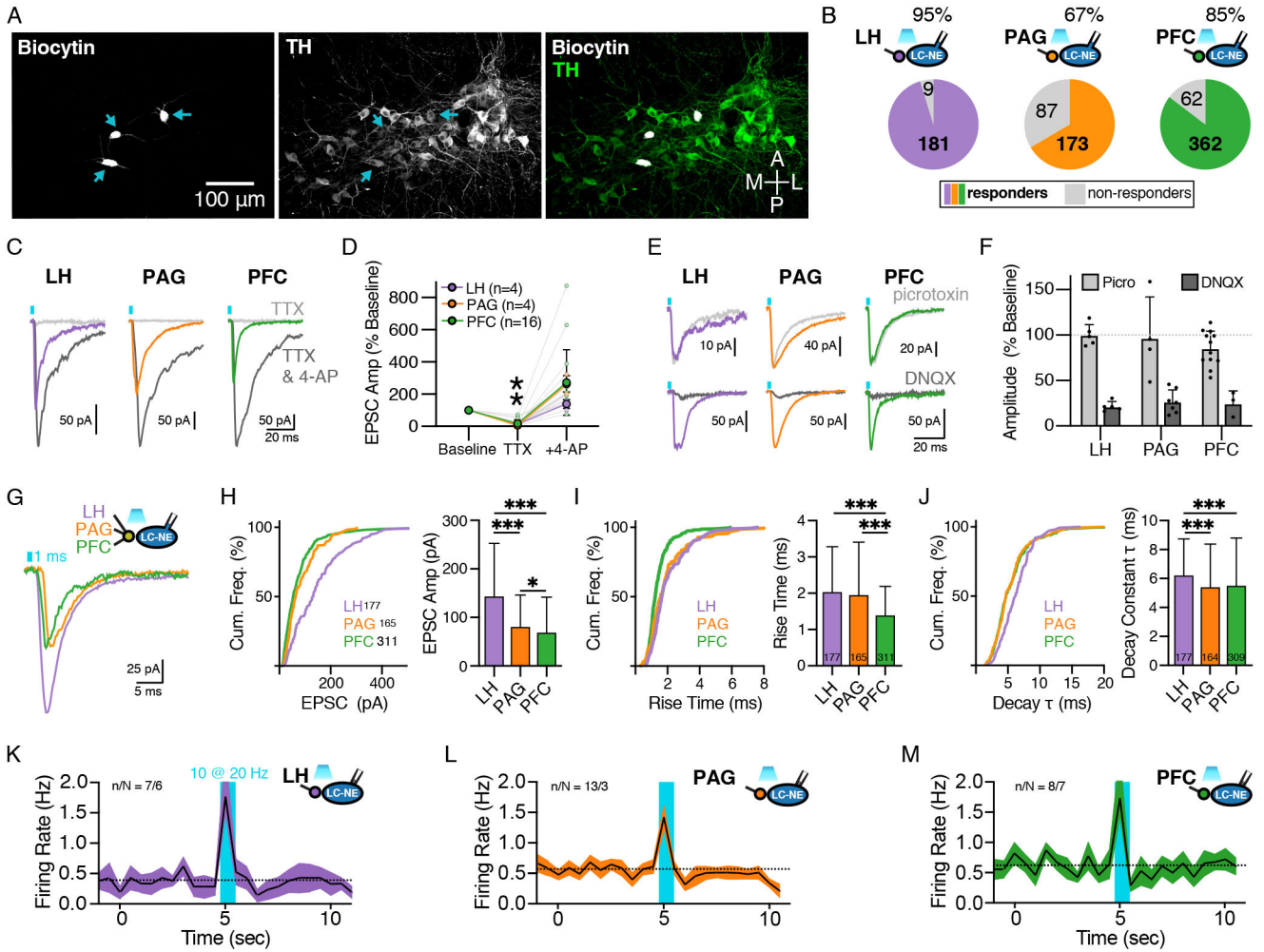


Figure 2. Synaptic properties of glutamatergic afferents from LH, PAG, and PFC to LC-NE neurons differ.

(A) Representative image of recorded LC-NE neurons filled with biocytin (left) and immunostained for TH (center); merged channels shown on right.

(B) Percent connectivity of LH, PAG, and PFC inputs with LC-NE cells. Number in the colored section represents cells with significant response and in the grey section represents cells with no measurable response. At 95% response rate, LH was significantly greater than PAG (67%) and PFC (85%), $\chi^2 = 67.80$, $p < 0.0001$.

(C) Representative traces in control, TTX (1 μ M), and TTX + 4-AP (0.5 mM).

(D) Quantification of EPSC amplitude in the presence of TTX and TTX + 4-AP normalized to baseline amplitude for LH (purple), PAG (orange) and PFC (green). Paired t-tests comparing normalized responses between TTX and TTX+4-AP were significant for all afferents such that 4-AP significantly rescued EPSCs.

(E) Representative traces of EPSCs recorded from LC-NE neurons with optogenetic stimulation of each afferent under control conditions and in the presence of picrotoxin (100 μ M) or DNQX (10 μ M).

(F) Quantification of EPSC amplitude in the presence of picrotoxin and DNQX normalized to baseline amplitude for each afferent.

(G) Representative traces for optically-evoked EPSCs from LH (purple), PAG (orange) and PFC (green) afferents.

(H) Quantification of EPSC amplitudes as a cumulative frequency distribution (top) and of the mean \pm SEM (bottom). Kruskal-Wallis ANOVA with posthoc Dunn's test, $H(2) = 88.36$, $p < 0.0001$; ***LH vs. PAG $p < 0.0001$, ***LH vs. PFC $p < 0.0001$, *PAG vs. PFC $p = 0.044$.

(I) Quantification of EPSC rise times as a cumulative frequency distribution (top) and of the mean \pm SEM (bottom). Kruskal-Wallis ANOVA with posthoc Dunn's test, $H(2) = 52.96$, $p < 0.0001$; LH vs. PAG $p = 0.3$, ***LH vs. PFC $p < 0.0001$, ***PAG vs. PFC $p = 0.0244$.

(J) Quantification of EPSC decay constants as a cumulative frequency distribution (top) and of the mean \pm SEM (bottom). Kruskal-Wallis ANOVA with posthoc Dunn's test, $H(2) = 22.54$, $p < 0.0001$; ***LH vs. PAG $p = 0.0003$, ***LH vs. PFC $p < 0.0001$, PAG vs. PFC $p > 0.99$.

(K-M) Firing rates of LC-NE neurons following optogenetic stimulation of LH, PAG or PFC afferents (20 Hz; 1 ms pulse; 0.5 sec duration; cell attached recordings) (K) Activation of ChR2 in LH afferents, $n/N = 7/6$. (L) Activation of ChR2 in PAG afferents, $n/N = 13/3$. (M) Activation of ChR2 in PFC afferents, $n/N = 8/7$.

Summary data are mean \pm SD. * = $p < 0.05$, *** = $p < 0.001$.

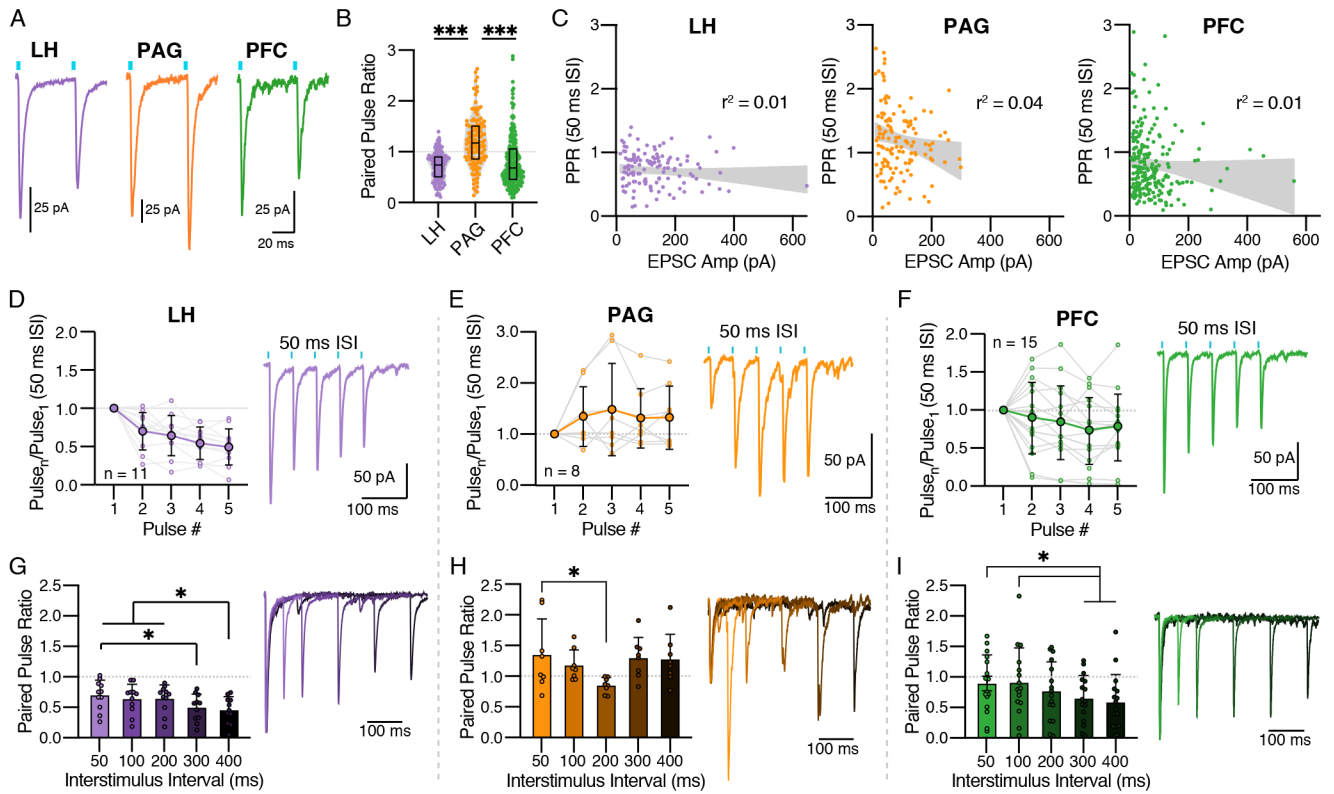


Figure 3. Glutamate release probability varies among LC-NE inputs.

(A) Representative traces showing paired pulse ratios (PPR) at a 50 ms interstimulus interval (ISI) for LH (left; purple), PAG (center; orange), and PFC (right; green).

(B) Quantification of paired pulse ratios at a 50 ms ISI (mean \pm SEM). Kruskal Wallis ANOVA with post-hoc Dunn's Test, $H(2) = 80.11$, $p < 0.0001$; ***LH vs. PAG $p < 0.0001$, LH vs. PFC $p = 0.87$, ***PAG vs. PFC $p < 0.0001$.

(C) Scatter plots showing the relationship between PPRs and EPSC amplitudes; the size of the response did not significantly account for variability in PPR.

(D-F) Quantification (left) and representative traces (right) for trains of 5 pulses with 50 ms ISIs. For each input a RMANOVA with post hoc Tukey's test was used to compare the ratio of pulse_n to pulse₁. (D) LH had a significantly lower ratio for pulses 4 and 5 as compared to pulse 2 ($F(4,40) = 19.70$, $p < 0.0001$). (E) PAG facilitated on all pulses with significant differences between them ($F(4,28) = 1.83$, $p = 0.15$). (F) PFC responses on average depressed for all pulses ($F(4,56) = 2.72$, $p = 0.0383$).

(G-I) Quantification (left) and representative traces (right) for PPRs of varying ISI (50 – 400 ms). For each input a RMANOVA with post hoc Tukey's test was used to compare PPRs. (G) LH inputs depressed at all ISIs, with $PPR_{300} < PPR_{50}$, $PPR_{400} < PPR_{50}$, PPR_{100} , & PPR_{200} ($F(4,40) = 5.93$, $p = 0.0008$). (H) PAG inputs facilitated at all ISIs except 200 ms, which was significantly less than 50 ms ($F(4,28) = 2.95$, $p = 0.0376$). (I) PFC inputs depressed for all frequencies with $PPR_{100} > PPR_{300}$ and PPR_{400} ($F(4,60) = 5.60$, $p = 0.0007$). Traces for each of the 5 ISIs are shown overlapped with their first peak normalized to 1; the shade of each trace corresponds to that in the bar graph, going from lightest to darkest with increasing ISI.

Summary data are mean \pm SD. * = $p < 0.05$, *** = $p < 0.001$.

Author Manuscript

Author Manuscript

Author Manuscript

Author Manuscript

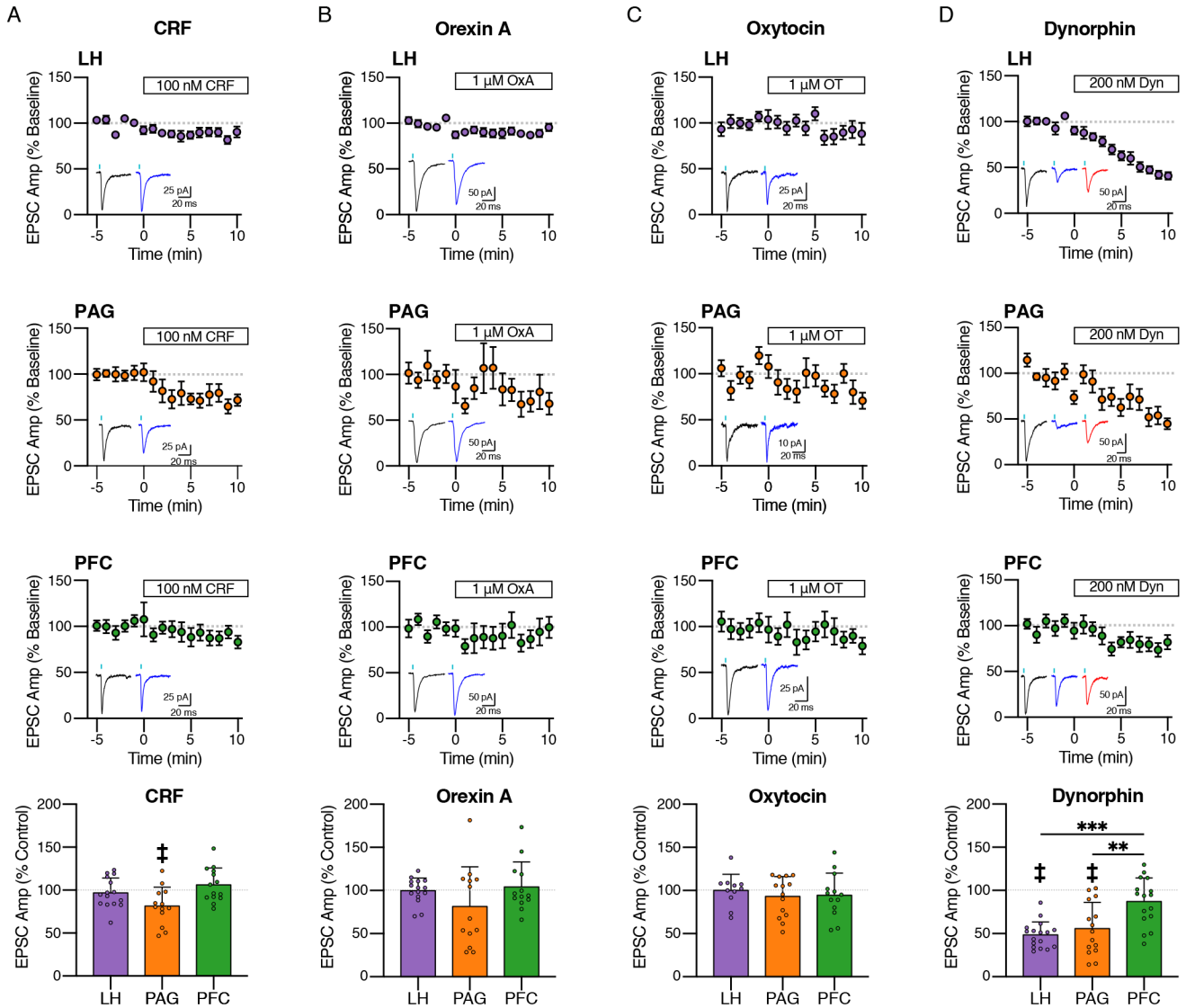


Figure 4. Peptidergic modulation of isolated afferents

(A) Effect of CRF (100 nM) on LH, PAG and PFC inputs. Quantification of average amplitudes normalized to baseline is shown for (A) LH (n = 15/9), (B) PAG (n = 9/8), and (C) PFC (n = 18/9), with representative traces of the last 5 minutes of baseline (black) and CRF (blue) to the right of the time course. Bottom: Quantification of the average EPSC amplitude after 6–10 minutes CRF application. CRF significantly reduced EPSC amplitudes only in PAG afferents ($18.58 \pm 21.94\%$ decrease, $t = 3.054$, $p = 0.01$).

(B) Effect of orexin A (OxA; 1 μ M) on LH, PAG and PFC inputs. Quantification of average amplitudes normalized to baseline is shown for (A) LH (n = 16/9), (B) PAG (n = 12/10), and (C) PFC (n = 13/8), with representative traces of the last 5 minutes of baseline (black) and OxA (blue) to the right of the time course. Bottom: Quantification of the average EPSC amplitude after 6–10 minutes OxA application.

(C) Effect of oxytocin (OT, 1 μ M) on LH, PAG and PFC inputs. Quantification of average amplitudes normalized to baseline is shown for (E) LH (n = 11/8), (B) PAG (n = 14/11),

and (C) PFC (n = 13/10), with representative traces of the last 5 minutes of baseline (black) and OT (blue) to the right of the time course. Bottom: Quantification of the average EPSC amplitude after 6–10 minutes OT application.

(D) Effect of dynorphin (Dyn, 200 nM) on LH, PAG and PFC inputs. Quantification of average amplitudes normalized to baseline is shown for (E) LH (n = 17/10), (B) PAG (n = 15/10), and (C) PFC (n = 16/11), with representative traces of the last 5 minutes of baseline (black) and Dyn (blue) to the right of the time course. Bottom: Quantification of the average EPSC amplitude after 6–10 minutes dynorphin application. LH and PAG amplitudes reduced significantly more than PFC (One Way ANOVA, $F(2,44) = 15.47$, $p < 0.0001$; Post-Hoc Tukey's Test, ***LH < PFC, ***PAG < PFC).

Time course data are mean \pm SEM. Summary data in bar graphs are mean \pm SD. ‡ = $p < 0.01$, ** = $p < 0.01$, *** = $p < 0.001$.